JIMMA UNIVERSITY

JIMMA INSTITUTE OF TECHNOLOGY, JiT

FACULTY OF MECHANICAL ENGINEERING

CHAIR OF THERMAL SYSTEM ENGINEERING

Design, Optimization and CFD analysis on the thermal performance of solar coffee dryer with jet impingement on corrugated absorber plate: The case of Limu coffee plantation

By: Ali Seid Hussen

A thesis submitted for the Partial Fulfillment of the requirements for the Degree of Master of Science in Thermal Systems Engineering

JIMMA, ETHIOPIA

May, 2019

JIMMA UNIVERSITY

JIMMA INSTITUTE OF TECHNOLOGY, JiT

FACULTY OF MECHANICAL ENGINEERING

CHAIR OF THERMAL SYSTEM ENGINEERING

Design, Optimization and CFD analysis on the thermal performance of solar coffee dryer with jet impingement on corrugated absorber plate:

The case of Limu coffee plantation

Advisors:

Main advisor: Balewgize A. Zeru (Asst. Professor)

Co-advisor: Debela Geneti (MSc.)

A thesis submitted for the Partial Fulfillment of the requirements for the Degree of Master of Science in Thermal Systems Engineering

JIMMA, ETHIOPIA

May, 2019

DECLARATION

I certify the work which is presented in dissertation entitled "**Design, Optimization and CFD analysis on thermal performance of solar coffee dryer with jet impingement on corrugated absorber plat: The case of Limu coffee plantation"** in partial fulfillment of the requirement for the award of Degree of Master of Science Thermal System Engineering submitted to faculty of mechanical engineering, Jimma institute of technology is my own work carried under the guidance and supervision of Balewgize A.(Asst.Prof.) and Debela G.(MSc.).

The matter contained in this dissertation has not been submitted neither in partial nor full to any other university or institute expect as reported in references.

Ali Seid	_____	_____
Done By	Signature	Date

Approved By

1. Balewgize A. Zeru (Asst. Professor)	_____	_____
Main Advisor	Signature	Date
2. Debela Genti (MSc.)	_____	_____
Co-Advisor	Signature	Date
3. _____	_____	_____
External Examiner	Signature	Date
4. _____	_____	_____
Internal Examiner	Signature	Date
5. Fikadu kifle (MSc.)	_____	_____
Thermal System Engineering Chair	Signature	Date

ACKNOWLEDGMENT

I am humbly grateful to **ALLAH** for guiding and helping me all the way through. Next, I would like to express my gratitude to my advisors; **Mr. Balewgize A. Zeru (Asst.Prof.)** and **Debela G. (MSc.)** for their support, contribution of ideas and effective comments during the whole study has provided me great ease at handling the problems that I have confronted. Next, I would like to thank my classmates and staff friends who were involved in this research. Next, I would like to express my deep gratitude to Jimma institute of Technology for giving this golden opportunity to attend MSc. program.

Finally, I must express my very profound gratitude to my parents for providing me with unfailing support and continuous encouragement throughout my years of study and through the process of researching and writing this thesis. This accomplishment would not have been possible without them.

ABSTRACT

In many countries of the world, the use of solar thermal systems in the agricultural area to conserve vegetables, fruits, coffee and other crops has shown to be practical, economical and responsible approach environmentally. Post-harvest drying of coffee is one of the main preservation techniques employed to enhance processing, storage quality, nutritional value, and market control. For these purposes, an efficient type of solar dryer is designed to dry Coffee. The modeling techniques are very important to develop analyses and predict the performance of a solar drying system. This paper presents study of computational fluid dynamics (CFD) based thermal efficiency analysis to determine heat transfer characteristics of solar air heater and drying chamber. Autodesk inventor professional is used to model the proposed design and Computational Fluid Dynamics code ANSYS FLUENT is used to simulate fluid flow and heat transfer. The design parameters considered in the analysis are solar collector without and with jet impingement, 6,8,10 mm jet diameters are used for jet impingement, 300 K ambient temperature, 0.02 – 0.05 kg/s mass flow rate, 500-800 W/m^2 of solar radiation of selected site and distribution of heated air in drying chamber by using front and back header.

The simulation results revels that the collector outlet temperature, Nusselt number, and thermal efficiency is more in D=6 mm jet diameter for mass flow rate of 0.05 and 600 W/m^2 solar radiation. The V-corrugated collector without jet plate has maximum efficiency of 64.3 %, and the maximum efficiency of 72.3% can be seen at jet diameter of 6 mm. The temperature distribution obtained was satisfactory due to the high uniformity inside the chamber by placing the front and back header in the drying chamber. For Loading rate of 50 kg coffee average drying rate is 4.12 kgH_2O/hr with drying efficiency of 38.5 %. Validation of results compared with previously performed experimental data from literature and found to be in good agreement. Collector efficiency predicted output with a deviation 8 %. Improvement in thermal efficiency of solar air heater is observed by using jet impingement on corrugate absorber plate. Solar collector with high performance and drying chamber with *good air flow distribution can improve the drying uniformity.*

Key Words: Solar Air Heater, Jet impingement, Heat Transfer, CFD, Coffee, Drying Chamber

Table of Contents

LIST OF TABLES

LIST OF FIGURES

LIST OF ABBREVIATIONS AND NOMENCLATURES

CFD	Computational Fluid Dynamics
EES	Engineering Equations Solver
SAH	Solar Air Heater
A	area of absorber plate (m2)
Cp	specific heat of air (J/kg K)
Dh	hydraulic diameter of the air flow path (m)
Dj	jet hole diameter (m)
f	friction factor of duct
g	acceleration due to gravity (m^2/s)
hc	convective heat transfer co efficient (W/m^2 K)
hc	convective heat transfer coefficient due to
hr	radiative heat transfer co efficient (W/m^2 K)
hw	wind (W/m2 K)
k	thermal conductivity (W/m K)
L	length of the duct (m)
ṁ	mass flow rate of air (kg/s)
N	total number of holes
Nu	Nusselt number
Qu	useful heat gain (W)
Re	Reynolds number
I	intensity of solar radiation (W/m^2)
T	temperature (K)
Ub	bottom loss coefficient (W/m^2 K)
Vw	wind velocity (m/s)
W	width of the collector
X	stream wise pitch (m)

Y	span wise pitch (m)
Z	height of the duct (m)
σ	Stefan's Boltzmann constant ($W/m^2 K^4$)
ε	Emissivity
α	absorptivity
τ	transmissivity of glass cover
μ	viscosity (kg/m s)
ρ	density (kg/m3)
η_{th}	thermal efficiency (%)
η_{eff}	effective (or) thermo hydraulic Efficiency
θ	tilt angle (°)
ΔP	pressure drop (N/m^2)

Subscripts

1	flow path under jet plate
2	flow path above jet plate
a	air inside the flow path
am	ambient air
bp	back plate
c	glass cover
i	inlet
in	insulation
j	jet plate
o	outlet
p	absorber plate
s	sky

CHAPTER ONE

1 INTRODUCTION

In our nature, we have an abundant amount of solar energy, which may be extensively used as an energy source. So among research community in the world, solar energy utilization for society has become one of the most important issues. A Solar air heater is one among solar thermal systems which are extensively used for heating purposes like drying of crops, space heating, winter home heating, seasoning of timber, etc. In many countries of the world, the use of solar thermal systems in the agricultural area to conserve vegetables, fruits, coffee, and, other crops has shown to be practical, economical and the responsible approach environmentally. Solar heating systems to dry food and other crops can improve the quality of the product while reducing wasted produce and traditional fuels.

In rural areas, the drying of agricultural products usually relies on direct exposure to sunlight. Obviously, this traditional method for the drying of agricultural products requires a long drying period and has sanitary problems that lower the quality of dried products. For mass production of agricultural products, it is essential to have a drying device or facility, but this greatly increases the cost of dried agricultural products due to high-energy consumption for the drying process.

Ethiopia is country receives abundant solar radiation which could be used for drying of agricultural products, space heating, and, air conditioning, industrial processes and greenhouse heating using solar air collector devices. The solar air collectors occupy an important place among solar heating systems because of availability, minimal cost and the direct use of air as the working substance reduces the number of required system components. However, the primary disadvantage of solar air collectors system is the need for handling relatively large volumes of air as a working fluid with low thermal capacity, poor thermal conductivity and the convective heat-transfer rate inside the air flow channel where the heated air is low, and a great deal of effort has been made to increase this rate. Many ways have been done to improve the convective heat transfer rate such as increasing the heat-transfer surface area and increasing the turbulence inside the channel by using fins, corrugated surfaces, obstacles, porous bed materials, and applied the recycle-effect concept in double-pass operations.[1]

Drying involves the extraction of moisture from the product by heating and the passage of air mass around it to carry away the released vapor. Under ambient conditions, these processes continue until the vapor pressure of the moisture held in the product equals that held in the atmosphere [2]. Thus, the rate of moisture desorption from the product to the environment and absorption from the environment are in equilibrium, and the crop moisture content at this condition is known as the equilibrium moisture content. Under ambient conditions, the drying process is slow, and in environments of high relative humidity, the equilibrium moisture content is insufficiently low for safe storage [2].The objective of the drying process is to reduce the moisture content of coffee grains, so that it retains its organoleptic properties intact and reduce the risk of coffee contamination with mycotoxins or be affected by a fungus, implying that the grain loses quality and is rejected by the customers. The initial moisture content of the coffee is about 55-60% and after drying the final moisture content should be around 12% (w.b.) and the drying should be even and homogenized to obtain the proper color, size and to get rid of pests for the longer storage time [3]

Air is commonly utilized as a heat transfer fluid in many types of energy conversion schemes. Almost any black surface ignited by the sun can transfer a high temperature for air when the air is blown up. Air is distributed over the black radiation-absorbing surface and the air stream should be in contact with the complete collector surface to reach the higher temperatures. The air collector is usually over-laid by one or more transparent covers to reduce the heat loss.

In recent decades, many researchers have developed various design and configurations of solar air heater to improve their performance. It has been shown that one of the effective ways to increase the convective heat transfer rate between absorber plate and flowing air is to increase the heat transfer surface area and to increase turbulence inside the flow channel by using fins or corrugated surfaces[4]. Different design and configurations of solar air heaters like fins and baffles on absorber, corrugated absorber, roughened absorber, and packed bed have been developed to improve their performance by various authors [5]

The thermal efficiency of solar air heaters has been found to be generally poor because of their inherently low heat transfer capability between the absorber plate and air flowing in the duct. In order to make the solar air heaters economically viable, their thermal efficiency needs to be improved by enhancing the heat transfer coefficient. The jet impingement concept is one of the effective methods for increasing the heat transfer coefficient in a solar dryer. A fluid flow impinged against a surface can efficiently transfer large amounts of thermal energy between the surface and the fluid.

The application of software is very important to develop and analyze the mathematical models and predicting the performance of different kind of solar drying systems. The design of solar drying can be optimized with the help of software and it saves time which consumed during experiments. It is also useful for predicting the crop temperature, moisture content and drying rate, drying kinetics, texture and color of the crop. Computational fluid dynamics (CFD) can be used for the analysis and investigation of air flow, air flow rate inside the solar dryer, temperature distribution pattern and humidity, through appropriate simulation of energy and momentum equations and heat and mass transfer in both gaseous and solid phases. In recent years CFD has been applied in the design of a solar air heater. The studies reported that the quality of the solutions obtained from CFD simulations are largely within the acceptable range proving that CFD is an effective tool for predicting the behavior and performance of a solar air heater. MATLAB is a very useful tool for developing mathematical models to predict the crop temperature, air temperature, the moisture evaporated and for predicting the thermal performance of the solar dryer. It is also very supportive of training and testing of various models [6].

This research deals numerical simulation of solar collector and drying chamber for increasing efficiency by analyzing heat transfer characteristics for inline arrays of circular jets on the corrugated absorber plate, through circular jets in a duct flow of solar air heater, and compared with conventional solar air heater on corrugated plate absorber using CFD.

1.1 Components of Solar Dryer

1.1.1 Solar Collector

(i) **Absorber Plate:** The material of absorber plate should have good thermal conductivity, sufficient tensile and compressive strength and should be corrosion resistant. Copper is generally preferred because of its extremely high conductivity and resistance to corrosion. Collectors are also constructed with materials like aluminum, steel, Galvanized Iron (GI) sheets, and various thermoplastics and metal ions.

(ii) **Cover Plate:** Cover plate or plates through which the solar energy must be transmitted is also an extremely important part of solar air heater. Purposes of cover plates are;

(a) To transmit the maximum amount of solar radiation possible to the absorber plate.

(b) To minimize the loss from the absorber plate to the environment.

(c) To shield the absorber plate from direct exposure to weathering.

(iii) **Insulation:** Insulations are provided to reduce heat loss from the absorber plate due to conduction or convection. Generally used insulating materials are glass wool or rock wool. Absorber plate should be insulated beneath and or in the side, depending on the type of design used. An important requirement of an insulator is that it should be heat resistant.

1.1.2 Drying Chamber

- ✓ The drying chamber is an enclosed structure where drying takes place. It will consist of trays for putting in the product to be dried. At the drying chamber, there should be means for loading and removing the material to be dried. This is usually provided by a door at the back side of the dryer. The drying chamber should be insulated and well-sealed in order to contain the heated air without any leaks. Application of tray dryer is widely used in agricultural drying because of its simple design and capability to dry products at high volume. The key to the successful operation of the tray dryer is uniform airflow distribution over the trays. Good airflow distribution will ensure the final moisture content of the dried products on the trays are uniform. However, the greatest drawback of

the tray dryer is uneven drying because of poor airflow distribution in the drying chamber. Implementing the proper design of a tray dryer system may eliminate or reduce non-uniformity of drying and increases dryer efficiency. Computational fluid dynamics simulation is a very useful tool in the optimization of the drying chamber configuration by predicting the airflow distribution and the temperature profile throughout the drying chamber. Optimization using CFD can produce a better performance of the tray dryer system, high quality of dried products and uniform drying at minimum cost.

1.2 Drying parameters

- ✓ Dry bulb temperature: The temperature of moist air specified by an ordinary thermometer.
- ✓ Wet bulb temperature: The temperature of moist air specified by a thermometer, the bulb of which is covered with a wet wick
- ✓ Dew point temperature: The temperature at which the condensation of water vapour begins if a mixture of air and water is cooled.
- ✓ Relative humidity: The ratio of water vapour pressure in the air to water vapour pressure of the saturated air.
- ✓ Humidity ratio: The weight of water vapour which is associated with unit weight of dry air.
- ✓ Enthalpy: The specific heat of air with water vapour content in it is known as the enthalpy of moist air.
- ✓ Moisture content: It is expressed as a percentage of moisture based on wet weight or dry matter.
- ✓ Equilibrium moisture content: The rate at which the product losses moisture to the surrounding environment is identical to the rate at which it absorbs moisture from the surrounding air, the product is said to be in equilibrium.
- ✓ Drying ratio: It is a dimensionless number representing the ratio of the weight of wet material entering a dryer to the weight of the same material leaving the dryer.
- ✓ Latent heat :This property is required to estimate the energy required for evaporation of the desired amount of water from wet product [7].

1.3 Classification of solar dryers

For solar drying systems, different types of dryers are used with different sizes and designs, that is depend on the application and requirements. Usually, solar dryers are classified according many factors [8].

- ✓ Air movement method,[active, passive or hybrid dryers]
- ✓ Solar contribution,[direct, indirect and mixed solar dryers]
- ✓ Air movement direction,[parallel, counter flow]
- ✓ Type of product to be dried.

1.4 PROBLEM STATEMENTS

Solar drying is one of the methods used for conserving agricultural products. The earlier investigators have shown that the drying is an energy-intensive operation, which involves the complex processes of heat and mass transfer between the product and the drying medium. The research performed so far on solar drying shows that in order to meet the increasing demands for drying of crops, especially, in developing countries like Ethiopia, simple, cheap and efficient solar dryers have to be developed. The evolution of a solar drying system goes on improving every year in leaps and bounds, based on agricultural needs. The earlier stage research was carried out in all general areas in solar air heating systems, but not developed broadly for improving the performance of the overall system.

The traditional method, still widely used throughout Ethiopia, is open sun drying for diverse crops, such as coffee, cereals, etc. are spread on the ground and turned regularly until sufficiently dried. However, large-scale production limits the use of open sun drying because it suffers from several drawbacks such as it requires long drying time and inability to control the drying process properly, uncertainties of weather, cost of labor, need for large areas, infection by insects and other foreign matter which leads high crop losses. The disadvantages of open sun drying need an appropriate technology that can help in improving the quality of the dried products and in reducing the wastage. This led to the application of various types of drying devices like the solar dryer, electric dryers, wood fuel driers, and oil-burned driers. However, the high cost of oil and electricity and their scarcity in the rural areas have made some of these driers very unattractive.

Drying is a critical aspect of coffee processing, since storage quality, nutritional value and market control of the coffee beans depends on how dry they are and also on the way in which they have been dried. For economic reasons, maximum drying rates are desired with considerable product quality. In a solar drying system, some of the specific techniques need to be improved to dry products rapidly, uniformly and hygienically. A properly designed solar dryer can alleviate the disadvantages of open sun drying and the quality of the final product can be improved. Therefore interest will be focused mainly on the development of efficient solar driers.

1.5 OBJECTIVES

1.5.1 General Objective

- The general objective of the study is to design, optimization and CFD analysis on the thermal performance of solar coffee dryer with jet impingement on corrugated absorber plate.

1.5.2 Specific Objectives

The specific objectives of this study are:

- To investigate the effect of jet impingement on the heat transfer enhancement solar air heater by numerical (CFD) analysis.
- To find out the collector and Dryer efficiency
- To find out the optimal configuration of inline jet impingement for the maximum heat transfer enhancement using CFD.
- To design a drying chamber with a better air distributor location.
- To validate with experimental results from the literature.

1.6 The Significance of the Research

This research has the following significance,

- ✓ Protection of the coffee product from insects, birds, dust, and rain.
- ✓ Reducetion of the grand postharvest losses.
- ✓ Long-term storage without deterioration.
- ✓ Production of the hygienic marketable coffee product.

1.7 The Scope of the Study

This research deals CFD simulation of the solar collector drying chamber and how to increase its efficiency by analyzing heat transfer characteristics for inline arrays of circular jets on the corrugated absorber plate by varying different geometrical parameters of the jet plate and heated air distribution in drying chamber. This research does not include mass transfer between coffee and heated air by ANSYS. Experimental and model fabrication tasks are not included in this thesis.

CHAPTER TWO

2. LITERATURE REVIEW

2.1 Research Studies

Many types of research have been concerned to study the improvements in solar dryer performance. They found that to improve the performance, several ways and methods may be used such as, using extended surfaces, heat storage materials and surface roughness has a great effect on the performance of solar dryer.

T. Raja Srinivasan et al [9] Experimental investigation on the performance of an impinging jet solar air heater. The study is focused on the parameters that affect the heat transfer characteristics and compared with conventional solar air heater. The system is examined by varying the angle of attack (0, 10, 20, 30, 60 and 90) and the nozzle diameter (3, 5 and 7) mm in the air mass flow rate range of 0.012–0.016 kg/s. The study revealed that the highest performance is achieved with the 30 angles of attack, and the lowest performance is recorded with the 0°. The reduction in jet diameter increases the pressure loss in the collector. The better system performance is observed with the 5 mm diameter hole. The maximum thermal enhancement factor of 2.19 and efficiency of 55.8% are reached with the flow rate of 0.016 kg/s.

Yadav et al. [10] Performed of an artificial roughness in the form of repeated ribs on a surface are an effective technique enhances the rate of heat transfer. A numerical investigation of the heat transfer and fluid flow characteristics of fully developed turbulent flow in a rectangular duct having repeated transverse square sectioned rib roughness on the absorber plate have been carried out. The commercial finite-volume CFD code ANSYS FLUENT (ver. 12.1) is used to simulate turbulent airflow through artificially roughened solar air heater. The Navier-Stokes equations and the energy equation are solved in conjunction with a low Reynolds number RNG k-e 3 turbulence model. Twelve different configurations of square sectioned rib (P/e ¼ 7.14 e 35.71 and e/D ¼ 0.021 e 0.042) have been considered. The flow Reynolds number of the duct varied in the range of (3800-18000) most suitable for solar air heater. It has been found that the square sectioned transverse rib roughened duct with P/e ¼ 10.71 and e/D ¼ 0.042 offers the best thermo-hydraulic performance parameter for the investigated range of parameters.

Cigdem Tiris et al [11] Designed and developed a forced convection solar dryer for drying sultana grapes, green beans, sweet peppers, and chili peppers. The helical type absorber of the dimension 0.57 mx2.03m used a solar collector, aluminum wires (1 to 1.5mmdiameter) painted black and a polyester plate containing glass wool as the transparent cover. The drying chamber dimensions were 0.51m x1.05 m 1.29m and an electrical heater was used to test the solar air heater, assisting in the selection of the proper inlet air temperature of the working fluid. The inlet temperatures ranged between $44.1^0$and 60.2^0, the outlet temperature ranged between $36.5^0$and 59.8^0 and the total radiation intensity was varied between 244.3W⁄m^2 and 864.8W⁄m^2. The drying time for sultana grapes, green beans, sweet pepper and chili pepper using solar dryers was 5, 2.5, 5 and 2.5 days respectively, while the open sun drying took 11, 9.5, 10.75 and 5.2 days respectively.

Sharma et al. [12] Experimentally investigated artificial roughness by using circular wires attached to an absorber plate in the duct of a double-pass SAH. The wires were arranged in a V-shape and had relative roughness heights and Reynolds numbers corresponding to ranges of 0.022–0.044 and 4900–12000, respectively. The values of the Nusselt number and friction factor for the roughened collector were compared with the corresponding values of the smooth duct. Considerable enhancements in Nusselt number and friction factor were reported. Similarly, he also investigated the effect of the roughness parameters of V-ribs in a double-pass SAH. The angle of attack, relative rib pitch, and relative rib height was considered as roughness parameters and had values corresponding to the following ranges: 5–10°, 30–75°, and 0.022–0.033, respectively. The maximum Nusselt number and friction factor were found at an angle of attack of 60°, relative rib pitch of 10 and relative rib height of 0.033 as reported. The maximum enhancement factor in Nusselt number and friction factor were reported as 1.7 and 1.9, respectively.

Nayak et al. [13] Studied the effect of geometrical aspects of jet plate solar air collector with varying parameters such as mass flow rate varied from 0.030 to 0.065 kg/s and 0.20 to 0.043 kg/s; Reynolds number varied from 2700 to 6900; depth ratio varied from 0.75 to 1.0. In their study, the performance of impinging jet solar thermal collector delivered higher efficiency compared to the conventional solar thermal collector.

T. Alam et al [14] Studied experimentally and theoretically, flat plate, finned and v-corrugated SAHs under the same operating conditions. It was found that the v-corrugated collector is 5–11% and 10–15 more efficient in a double pass and single pass modes, respectively, compared with flat plate collectors. Also, the efficiency of all three collectors increased with increasing mass flow rate and saturated beyond a flow rate of 0.056 kg/ s. For double pass mode, the improvement in efficiency was most significant in the flat plate collector and small in the v-groove collectors.

Omojaro et al [15] investigated experimentally thermal performance of a double and single-pass SAH with fins attached and utilizing a steel wire mesh as absorber plate. It was found that for the same flow rate, the efficiency of the double pass is found to be higher than that of the single pass by 7–19.4%. Maximum efficiency obtained for the double and single pass SAH was 63.74% and 59.62%, respectively. Moreover, the efficiency further decreases with increasing the height of the first pass of the double pass SAH. In addition, their results revealed that using steel wire mesh arrange in layers as an absorber plate and packing material indicated a much more substantial enhancement in the efficiency. The effect of mesh height and number was not taken into consideration.

Karima et al [16] studied experimentally and theoretically flat plate, finned and v-corrugated SAHs under the same operating conditions. It was found that the v-corrugated collector is 5–11% and 10–15 more efficient in a double pass and single pass modes, respectively, compared with flat plate collectors. Also, the efficiency of all three collectors increased with increasing mass flow rate and saturated beyond a flow rate of 0.056 kg/ s. For double pass mode, the improvement in efficiency was most significant in the flat plate collector and small in the v-groove collectors.

Metwally et al. [17] analyzed a corrugated duct SAH and other five conventional designs. The enhancement factor of the convective heat transfer coefficient within the corrugated duct was 4-5. It was also confirmed that the heat removal factor of the corrugated duct collector had improved by an average value of 59%, while its efficiency had been enhanced by 15–43% over the other conventional collectors at a flow rate range of 0.01–0.1 kg/sm2 and solar insolation of 950 W/m2. They concluded that the corrugated duct SAH can be regarded as an advanced design that is priced similar to conventional designs.

Shi et al. [18] Presented simulation results for a single semi-confined turbulence slot jet impinging normally on a flat plate. The effects of turbulence models, near wall treatments, turbulence intensity, jet Reynolds number, as well as the type of thermal boundary condition on the heat transfer, were studied using the standard k-ε and RSM models. Their results indicate that both standard k-ε and RSM models predict the heat transfer rates inadequately, especially for low nozzle-to-target spacing. For wall-bounded flows, large gradients of velocities, temperature and turbulence scalar quantities exist in the near wall region and thus to incorporate the viscous effects it is necessary to integrate equations through the viscous sub-layer using finer grids with the aid of turbulence models.

Khalifa A.J.N.et al [19] An indirect mode forced solar dryer to dry the fruit and vegetable in Iraq has been constructed and tested. The drying system consisted of three main components are a solar collector, a blower and drying chamber. Two air solar collectors with V-groove absorbers, two air passes, and single glass cover was used. The total area of collectors absorber is 2.4 m2.The drying chamber dimensions are width = 1 m, depth = 0.33 m and height = 2 m. The chamber has six separated trays separated by five shelves with 0.3m except for the upper one, which is 0.5 m from the roof. Drying chamber walls are made from aluminum plate except for the southern side, which was fixed with a glass plate. Many types of products were used such as grapes, apricots, and beans. The results of this study showed that apricots moisture content reduced from 80% to 13% within 1.5 days of drying, grapes moisture content has been reduced from 80% to 18% in 2.5 days of drying and the beans have been reduced from 65% to 18% in 1 day only. The researchers showed that air temperature is the most effective factor in drying rate. The effect variation of airspeed inside the drying chamber was very small, so can be neglected. Additionally, the relative humidity of output air from the chamber was low between 25 and 30% and therefore there is no need for high-velocity air inside the drying chamber.

Romero V.M. et al [20] CFD fluent program used to simulate vanilla drying process by indirect solar dryer prototype. The simulated model has been validated with experimental results. Drying system consisted of a flat solar collector with dimensions (2.0 m×1.0 m×0.1 m), drying cabinet with dimensions (1.0 m×0.80 m×1.2 m) and 1.2 m chimney with diameter 0.2 m. Solar dryer geometry was made with ANSYS design modeler program with 21° tilt angle of with respect to the horizontal plane was considered for the months from January to

March. Comparison between CFD simulated and thermal measured results showed that at solar collector outlet there was a good degree of similarity between measured and calculated temperatures. For drying tests have been obtained 62% reduction in weight, this was a very good reduction in time compared with the time required for the traditional process.

Mohanraj M. et al.[7] An indirect mode forced convection solar dryer integrated with different sensible heat storage material for copra drying had been developed. The drier consists of a solar flat plate air collector provided a heat storage unit, a drying chamber and a centrifugal type blower as shown in

. The experiments have done with and without the integration of heat storage materials. Sand mixed with aluminum scrap was used as a heat storage material in solar air collector. The results showed the specific moisture extraction rate of the solar dryer was estimated to be about 0.81 and 0.94 kg kW/h in cases the solar air collector with and without heat storage materials respectively. The results proved also, the time to reduce the moisture content of copra from about 52% to about 8% with heat storage materials was about 80 hour, which is mean faster than without using storage materials with drying time 104 hour. The average thermal efficiency of the solar drying system with both drying modes was estimated to be about 23%. The indirect forced convection solar drier integrated with heat storage material is more suitable for producing high-quality copra, as can be seen in Fig. [7].

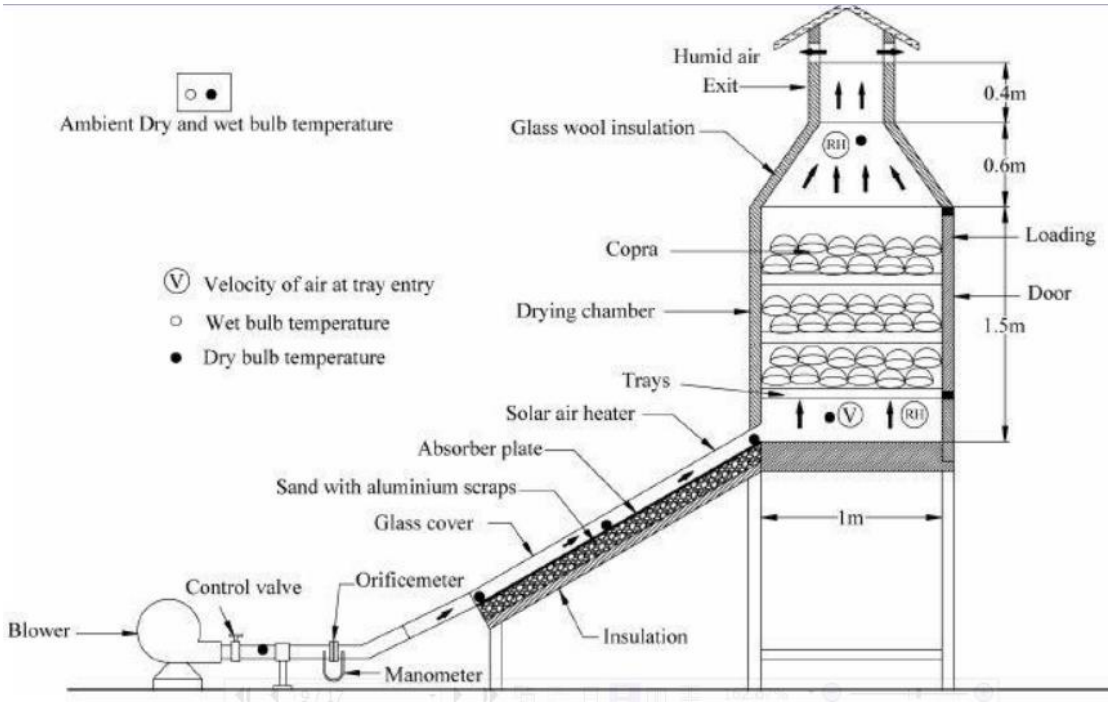

Figure 2. 1 *Indirect active solar dryer* [7]

P. Krawczyk *et al.* [21] Designed and developed a re-circulatory cabinet dryer using a central air distribution system. The capacity of the dryer is 5 kg/batch. Hot air is fed from the center to avoid non-uniform drying and to reduce the heat loss to the surroundings. A blanched potato chip was tested in the dryer. The results show that the velocity of both chambers is in the range of 1.5 m/s to 1.7 m/s. The initial heating time of air is 25 min and 12 min with no re-circulation and 100% re-circulation, respectively. The experiments were conducted at loading capacities of 5, 6 and 7 kg/m of potato chips and drying temperatures of 55, 60 and 65°C. The thermal heat efficiency and the heat utilization factor are in the range of 21% to 24% and 17% to 20%, respectively. The drying times of different loading capacities are in the range of 180 min to 225 min. drying products with a loading capacity of 7 kg/m are more economic because product quality is maintained despite differences in loading capacity.

Gülþah Cakmak et al. [22]designed and constructed an air solar collector with swirl flow to dry seeded grape. Additional air-directing elements on the wall of the drying chamber and a swirl element at the inlet of the drying chamber produced a uniform flow of drying air over the grapes on a single tray and the dried products reached the desired moisture conditions more rapidly than the products subjected to open sun drying. The drying time of 200 h under the open sun was decreased to 80 h with the developed dryer. The dryer air velocity was about 1.5 m/s. The drying rate increased with the increase in dryer air velocity. Thus, air velocity has a more significant effect on the drying process than does air temperature.

Karwa et al. [23] presented a study of the performance of SAH with 60^{o} v-down rectangular cross/section repeated rib on roughness on air flow inside of absorber plate. A detailed work has been exercised out using a mathematical model for study the effects of ambient, operating & design parameters on the thermal efficiency & effective efficiency in such air heaters. This study shows that air mass flow rates are less than about 0.04 kg s-1 per m2 from the absorber plate, & roughened duct SAH provide significant performance merit over smooth duct air heaters. The thermal & effective efficiencies differ minutely at low flow rates. Due to the increase in flow rate, the difference between the thermal & effective efficiencies increases because of the increase in the pumping of power. When the mass flow rate is about 0.045 kg s-1 m-2 the effective efficiencies of roughened & smooth duct SAH are actually the same.

A. Boulemtafes et al [24] proposed a two-dimensional CFD model of a SAH with an equilateral triangular sectioned rib roughness on the absorber plate. The study concerned with the impact of three parameters on the thermos-hydraulic performance of a roughened heater: relative roughness pitch, relative roughness height and Reynolds number (Re). The results showed that the average Nusselt number has the tendency to increase with the increase of Renolds number in all cases but the average friction factor decreases. On the other hand, average Nusselt number and the average friction factor decrease with the increase of relative roughness pitch at a fixed value of relative roughness height and increase as relative roughness height increases at a fixed value of relative roughness pitch. It is found that for the height of relative roughness of 0.042 and pitch of relative roughness of 7.14, the maximum Nusselt number and friction factor enhancement occurred at Re of 15,000 and 3800, respectively. The maximum enhancement of Nusselt and friction factor enhancement over a smooth duct was found to be 3.073 times and 3.356 times, respectively. The value of the thermohydraulic performance parameter varies between 1.36 and 2.11 for the range of parameters investigated.

In conclusion, substantial experimental and analytical research has been conducted on extended surfaces such as fins, wires, corrugated absorbers, longitudinal fins, cross, and non-cross flow inline jet plate solar air heaters have been used to enhance the convective heat transfer coefficient and outcomes have been implemented for different flow configurations. But, So far, very few studies are available on forced jet impingement at corrugated plate solar dryer and more work is required to investigate this technique because it offers superior thermal performance.

2.2 Summary of Related Works

Table 2. 1 **Summary of the literature review**

Authors	Year	Proposed work	Methodology	Result obtained	Validation
T. Raja Srinivasan [9]	2017	Investigation of the performance of an impinging jet solar air heater	The varying angle of attack (0, 10, 20, 30, 60 and 90) and nozzle diameter (3, 5 and 7) mm. For an air mass flow rate range of 0.012–0.016 kg/s.	Highest performance is achieved with the 30 angles of attack, and the lowest performance is recorded with the 0°. Reduction in jet diameter increases the pressure loss in the collector. Better system performance is observed with the 5 mm diameter hole. The maximum thermal enhancement factor of 2.19 and efficiency of 55.8% are reached with the flow rate of 0.016 kg/s.	Experimental
Sharma et al. [25]	2012	Experimentally investigated artificial roughness by using circular wires attached to an absorber plate in the duct of a double-pass SAH.	The angle of attack, 5–10°, Relative rib pitch 30–75° Relative rib height 0.022–0.033m were considered as roughness parameters. The nusselt number and friction factor were compared with the corresponding values of the smooth duct.	The maximum Nusselt number and friction factor were found at • an angle of attack of 60° • relative rib pitch of 10 • Relative rib height of 0.033. The maximum enhancement factor in Nusselt number and friction factor were reported as 1.7 and 1.9, respectively.	Experimental

Karima and Hawlader [16]	2006	The improvement in efficiency of the solar air heater	Studied flat plate, finned and v-corrugated SAHs under the same operating conditions for double and single pass	It was found that the v-corrugated collector is 5–11% and 10–15 more efficient in a double pass and single pass modes, respectively, compared with flat plate collectors. The efficiency of all three collectors increased with increasing mass flow rate and saturated beyond a flow rate of 0.056 kg/s. For double pass mode, the improvement in efficiency was most significant in the flat plate collector and small in the v-groove collectors.	Experimental and Theoretical
Yadav and Bhagoria [10]	2014	Two-dimensional CFD model of a SAH with an equilateral triangular sectioned rib roughness on the absorber plate	The study concerned with the impact of three parameters on the thermos-hydraulic performance of a roughened heater: relative roughness pitch, relative roughness height and Reynolds number (Re).	The average Nusselt number has the tendency to increase with the increase of Re all cases but the average friction factor decreases. The average Nusselt number and the average friction factor decrease with the increase of relative roughness pitch at a fixed value of relative roughness height It is found that for the height of relative roughness of 0.042 and pitch of relative roughness of 7.14, the maximum Nusselt number and friction factor enhancement occurred at Re of 15,000 and 3800, respectively.	Analytical with ANSYS simulation

Omojaro and Aldabbagh [15]	2010	Thermal performance of a double and single-pass SAH.	Double and single-pass SAH with fins attached and utilizing a steel wire mesh as absorber plate.	It was found that for the same flow rate, the efficiency of the double pass is found to be higher than that of the single pass by 7–19.4%. Maximum efficiency obtained for the double and single pass SAH was 63.74% and 59.62%, respectively. Using steel wire mesh arrange in layers as an absorber plate and packing material indicated a much more substantial enhancement in the efficiency.	Experimental
Tesfaye[26]	2016	Study on Solar Tunnel Dryer Mathematical Modeling and Simulation for Coffee Drying in Harar.	mathematical modeling and simulation	The parchment coffee exposed to the drying air gets dried faster than the parchment coffee found at the center.	Analytical
Aklilu[27]	2010	Simulation and Experimental Investigation on Active Solar Coffee Dryer	Mathematical, Experimental testing and ANASYS Simulation model	The moisture content of the coffee was reduced from 29% to 12.3% after 5h for clear sunshine day and average thermal efficiency of the dryer was determined to be 50.5% for clear sunshine day.	Experimental and Theoretical

CHAPTER THREE

3. METHODOLOGY

3.1 Study Area

The area selected for a present research study is Limu coffee plantation.

3.2 Data Collection

3.2.1 Meteorological Data

Limmu Coffee Farm located in the Oromia Regional State is geographically found in the most ideal coffee-producing area of the country. It lies around Jimma town, in Jimma Zone about 350 km West of Addis Ababa. The farm covers a total land area of 12,114 hectares of which nearly 8,000 hectares is covered with coffee. Currently, Limmu Coffee Farm produces and supplies over 5000 MT of distinctly unique, traceable, and high quality washed and sundried coffee to the world market. The region situated at a latitude of 8.06°N and longitude 36.57°E with an **elevation** of 1773 meters above sea level [27].

3.2.2 Solar Radiation

Global irradiation, ambient temperatures, and wind speed are the important meteorological parameters which influence the collector and drying chamber performance to a considerable extent. Solar Irradiance is a measure of how much solar power you are getting at your location. This irradiance varies throughout the year depending on the seasons. It also varies throughout the day, depending on the position of the sun in the sky, and the weather [28]. Solar insolation is a measure of solar irradiance over of period of time - typically over the period of single day Matlab models are used to establish a mathematic model of hourly solar radiation on the tilted surface at limmu, Ethiopia.

3.2.3 Basic Solar Components

3.2.3.1 Latitude (φ)

The latitude of an area is the position with relevance north or south of the Equator. The variation of the latitude is from 0◦ to ±90◦ (positive for northern and negative for the southern hemisphere), 0◦ at the Equator and ±90◦ at the Poles[29].

3.2.3.2 Declination Angle (δ)

Declination is the angular distance from the sun north or south to the earth's equator. Declination ranges between 23.45◦ north and 23.45◦ south. The northern hemisphere is inclined 23.45◦ far away from the sun sometime around 21 December, which is the summer solstice for the southern hemisphere and the winter solstice for the northern hemisphere. In the northern hemisphere and through 21 June, starting around 21 June, the southern hemisphere is positioned in a way that it is 23.45◦ away from the sun; meanwhile, it is winter solstice in the northern hemisphere. During the fall and spring equinoxes, which begin on 21 March and 21 September respectively, the sun passes directly over the equator. [30]

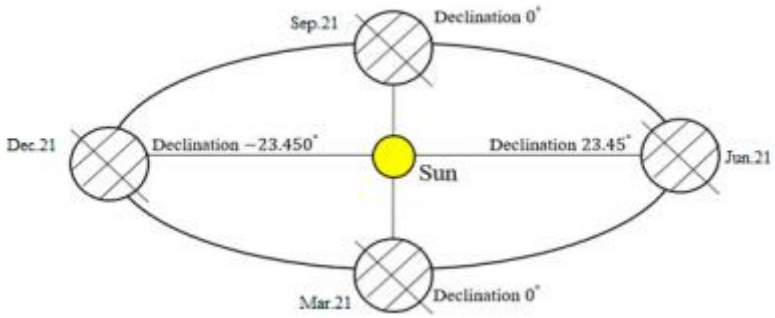

Figure 3. 1 Maximum and minimum value of declination angle [30]

$$\delta = 23.45°\sin(360°(284+n)/365) \quad (3.1)$$

3.2.3.3 Hour Angle (ω_s)

The concept of hour angle is used for describing the rotation of the earth around its polar axis which is equivalent to +15◦ per hour during the morning and −15◦ in the afternoon. It is the angular distance between the observer's meridian and the meridian whose plane contains the sun (**Error! Reference source not found.**). The following equation can be used to calculate the hour angle in degrees. It should be noted that at noon the hour angle ω is zero [30].

$$\omega_s = \cos^{-1}(-\tan\phi\tan\delta) \quad (3.2)$$

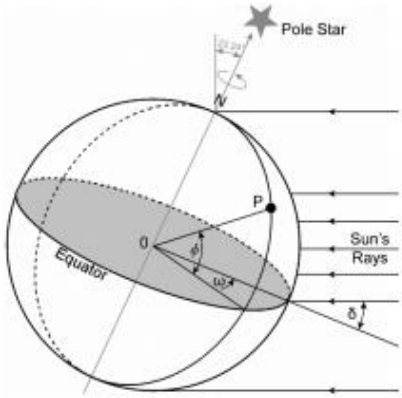

Figure 3. 2 **Hour angle (ω) for point P** [30]**.**

3.2.3.4 Solar Azimuth Angle (γ)

The angular displacement from the south of the beam radiation projection on the horizontal plane is defined as the solar azimuth angle. This is schematically illustrated in Figure below

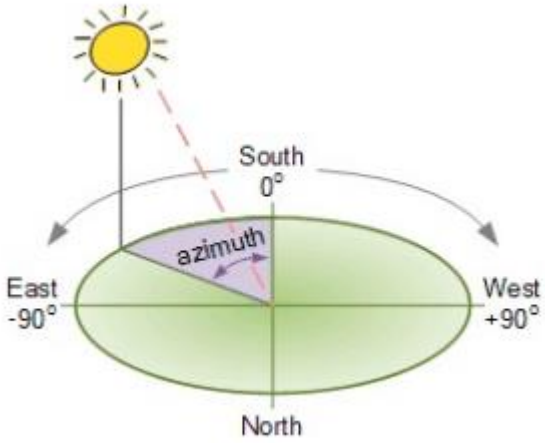

Figure 3. 3 Definition of sun's azimuth angle.[31]

3.2.3.5 Collector Orientation

The solar collector was tilted and oriented in such a way that it receives maximum solar radiation during operation. The best stationary orientation is due South in the northern hemisphere and due north in Southern hemisphere [25]. The angle of tilt (β) of the solar collector is given by the formula below [25];

$$\beta = 10^0 + Lat\phi \qquad (3.3)$$

Where; LatΦ = the latitude of the collector location = 8.06^0 for the selected site. Therefore, solar collector is oriented facing south and tilted at 18.06^0 which is the best recommended orientation for stationary absorbers. This inclination also allows easy run-off and enhance air circulation[32].

3.2.4 Hourly Global Solar Radiation on the Horizontal Surface

Extraterrestrial solar radiation

A simple equation of the extraterrestrial radiation with accuracy adequate for most engineering calculations is given by

$$G_{on} = G_{sc}\left[1 + 0.033\cos(360°n/365)\right] \quad (3.4)$$

Where G_{on} is the extraterrestrial radiation on the plane normal to the radiation on the *n*th day of the year, G_{sc} is the solar constant 1367W/m^2, n is a day of the year. Thus $0 \leq n \leq 365$.

Extraterrestrial radiation on a horizontal surface

The extraterrestrial solar radiation on a horizontal surface is calculated from [33]

$$H_0 = \frac{24\times 3600 G_{on}}{\pi}(\cos\phi\cos\delta\sin\omega_s + \frac{\pi\omega_s}{180^\circ}\sin\phi\sin\delta) \quad (3.5)$$

Where ϕ the local geographic latitude, δ is is the solar declination which range is ± 23.45 °, ω_s is the sunset hour angle, and generally considered the sunrise and sunset times are symmetrical.

3.2.5 Monthly Average Daily Solar Radiation on the Horizontal Surface

The Angstrom regression equation related monthly average daily radiation on extraterrestrial radiation is given by

$$\overline{H} = \overline{H_0}(a + b\frac{\bar{n}}{\bar{N}}) \quad (3.6)$$

$$a = -0.110 + 0.235\cos\phi + 0.323\left(\frac{\bar{n}_s}{\bar{N}_s}\right) \qquad b = 1.449 - 0.533\cos\phi - 0.694\left(\frac{\bar{n}_s}{\bar{N}_s}\right)$$

where $\overline{H}$ is the monthly average daily radiation on the horizontal surface, $\overline{H_0}$ is the monthly

average daily extraterrestrial solar radiation, with the value of $\bar{n}$ given in **Table 3.1**, a, b are empirical coefficients, $\bar{n}$ is the monthly mean daily sunshine duration, $\overline{N}$ is the monthly mean maximum possible sunshine duration, which can be calculated using

$$\overline{N} = \frac{2}{15}\omega_s \tag{3.7}$$

Table 3.1 Recommended average days for months and the values of n and $\bar{n}$ by months [33]

Month	n for *i*th Day of Month	Every day of Month		$\bar{n}$
		Date	n	
Jan.	i	17	17	6.4
Feb.	31+i	16	47	7.2
Mar.	59+i	16	75	7.7
Apr.	90+i	15	105	8.5
May	120+i	15	135	9.0
June	151+i	11	162	8.5
July	181+i	17	198	7.0
Aug.	212+i	16	228	7.5
Sept.	243+i	15	258	8.2
Oct.	273+i	15	288	7.5
Nov.	304+i	14	318	6.1
Dec.	334+i	10	344	5.9

Daily global solar radiation on the horizontal surface

$$H = \begin{cases} H_0(0.14 + 0.47\dfrac{\bar{n}}{N}) & (1 \leqslant n \leqslant 59, 305 \leqslant n \leqslant 365) \\ H_0(0.24 + 0.4\dfrac{\bar{n}}{N}) & (152 \leqslant n \leqslant 243) \\ H_0(0.36 + 0.23\dfrac{\bar{n}}{N}) & (60 \leqslant n \leqslant 151, 244 \leqslant n \leqslant 304) \end{cases} \tag{3.8}$$

The clearness index of a day K_T is given by

$$K_T = \begin{cases} 0.14 + 0.47\dfrac{\bar{n}}{N} & (1 \leqslant n \leqslant 59, 305 \leqslant n \leqslant 365) \\ 0.24 + 0.4\dfrac{\bar{n}}{N} & (152 \leqslant n \leqslant 243) \\ 0.36 + 0.23\dfrac{\bar{n}}{N} & (60 \leqslant n \leqslant 151, 244 \leqslant n \leqslant 304) \end{cases} \tag{3.9}$$

When hourly performance calculations for a system are to be done, it may be necessary to start with daily data and estimate hourly values from daily numbers [30].

The hourly total solar radiation on the horizontal surface

$$I = \frac{\pi H}{24}(0.409 + 0.5016\sin(\omega_s - 60^\circ) + (0.6609 - 0.4767\sin(\omega_s - 60^\circ))\cos\omega)\frac{\cos\omega - \cos\omega_s}{\sin\omega_s - (\frac{2\pi\omega_s}{360^\circ})\cos\omega_s} \tag{3.10}$$

Where ω_s is the hour angle in degrees for time (i.e., the midpoint of the hour for which the calculation is made), which can be computed [34]

$$\omega = 15\cdot((h + 9.87\sin(\frac{2\cdot 360(n-81)}{364}) - 7.53\cos(\frac{360(n-81)}{364}) - 1.5\sin(\frac{360°(n-81)}{364}) - 4(120\text{-}L_{LOG}))/60 - 12) \tag{3.11}$$

Where h is the limmu time, L_{LOG} is the local geographical longitude.

5.2.6 Hourly Diffuse Solar Radiation on the Horizontal Surface

The hourly diffuse solar radiation on the horizontal surface is given by [34]

$$I_d = \frac{\pi H_d}{24}\frac{\cos\omega - \cos\omega_s}{\sin\omega_s - (\frac{2\pi\omega_s}{360^\circ})\cos\omega_s} \tag{3.12}$$

Where H_d is the daily diffuse solar radiation on the horizontal surface, which can be obtained by

$$\frac{H_d}{H} = \begin{cases} 0.99 & (K_T \leqslant 0.17) \\ 1.188 - 2.272K_T + 9.473K_T^2 - & \\ 21.865K_T^3 + 14.648K_T^4 & (0.17 < K_T < 0.75) \\ -0.54K_T + 0.632 & (0.75 < K_T < 0.80) \\ 0.2 & (K_T \geqslant 0.80) \end{cases} \tag{3.13}$$

3.2.7 Hourly Global Solar Radiation on the Tilted Surface

The ratio of beam radiation on the tilted surface to that on a horizontal surface

Order to maximize the solar energy, it is necessary to ensure that the normal of the collector is in a straight line with the sun on the conditions of the brightest sunshine. So collectors should be placed toward the south in the northern hemisphere, which means the azimuth of the collector is equal to zero. The geometric factor R_b, the ratio of beam radiation on the tilted surface to that on a horizontal surface at any time, can be calculated [34]

$$R_b = \frac{\cos\theta}{\cos\theta_z} = \frac{\cos(\phi-\beta)\cos\delta\cos\omega + \sin(\phi-\beta)\sin\delta}{\cos\phi\cos\delta\cos\omega + \sin\phi\sin\delta} \tag{3.14}$$

Where θ the angle of incidence of the sun is, θ_z is the zenith angle of the sun, that is, the angle between the vertical and the line to the sun. When collector inclination β is equal to the local geographical latitude φ

$$R_{b,ave} = \frac{\cos\delta(\sin\omega_2 - \sin\omega_1)}{e+f} \tag{3.15}$$

Where

$$e = \cos\beta\cos\delta(\sin\omega_2 - \sin\omega_1) \tag{3.16}$$

$$f = \sin\beta\sin\delta\frac{\pi}{180}(\omega_2 - \omega_1) \tag{3.17}$$

ω_1 to ω_2 are a time period

3.2.8 The Ratio of Diffuse Radiation on the Tilted Surface to That on a Horizontal Surface

The diffuse solar radiation on tilted surface consists of two parts: the diffuse radiation from the sky and the ground-reflected radiation. A view factor to the sky R_d and a view factor to the ground are computed by [34]

$$R_d = \frac{1+\cos\beta}{2} \tag{3.18}$$

$$R_\rho = \frac{1-\cos\beta}{2} \tag{3.19}$$

Hourly global solar radiation on the tilted surface

At weather stations, the global solar radiation is generally measured on horizontal surfaces. Hourly global solar radiation on inclined surfaces can be estimated from global solar radiation on horizontal surfaces using several models. The models can be used to estimate components of hourly global solar radiation on horizontal surfaces (for direct and diffuse radiation) and inclined surfaces (for direct, diffuse, and ground-reflected radiation).[35]

The radiation on the tilted surface was considered to include three components: beam, isotropic diffuse and solar radiation diffusely reflected from the ground [34]. It can be computed by

$$I_T = I(\rho_g R_\rho + R_{b,\ \text{ave}}) + I_d(R_d - R_{b,\ \text{ave}}) \tag{3.20}$$

Where ρ_g is the ground albedo with 0.2 for ground and 0.7 for snow

The simulation of the solar radiation on the horizontal and tilted surface for a year has been carried out with programming language MATLAB. The duration of the simulation was set to be 8760 h and the time step of the simulation was 1 h. Model inputs parameters supplied are latitude, longitude, albedo, solar constant, and solar radiation data on a horizontal surface from the selected site. The outputs of the simulation include the global and diffuse radiation on a horizontal and tilted surface, the ratio of beam radiation on the tilted surface to that on a horizontal surface

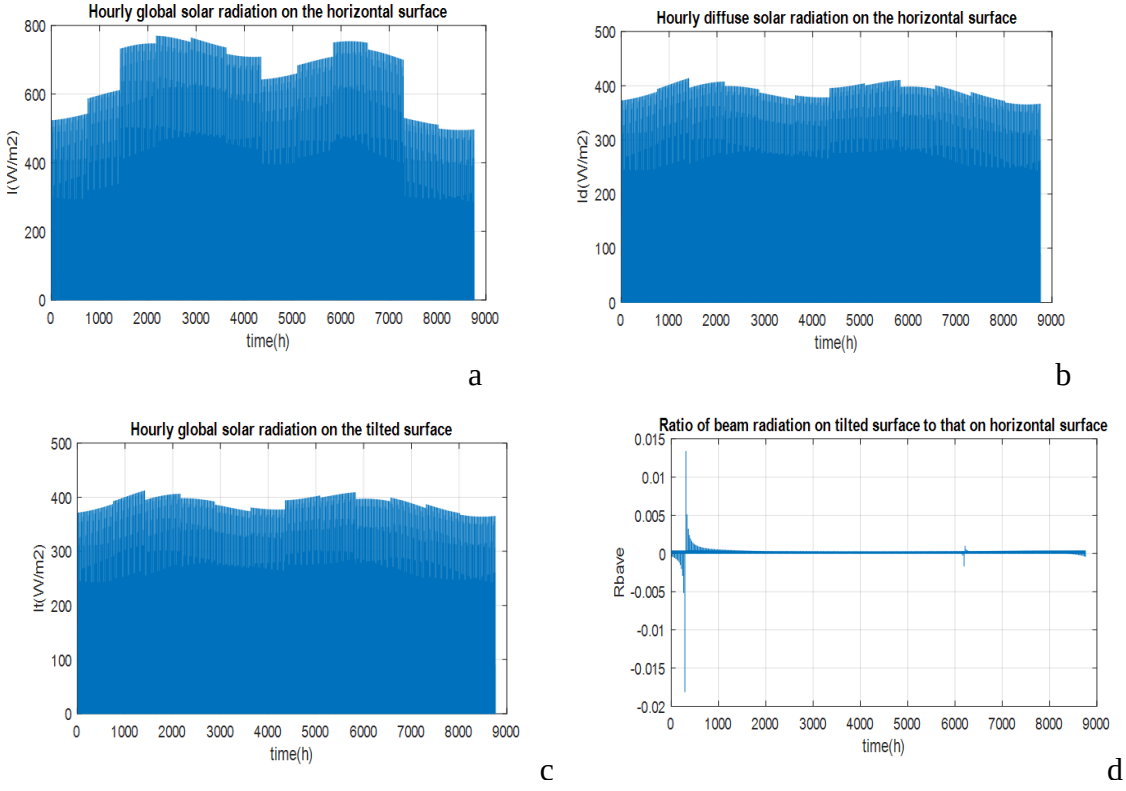

Figure 3. 4 **Solar radiation results.**

(a)Hourly global solar radiation on the horizontal surface for a year (b)Hourly diffuse solar radiation on the horizontal surface for a year (c)Hourly global solar radiation on the tilted surface for a year (d)Average ratio of beam radiation on the tilted surface to that on a horizontal surface for a year .

Table 3.2 Physical and fluid-dynamic properties of parchment coffee [3]

Property	Value
Thermal conductivity (W/m K)	0.13
Thermal diffusivity ($x10^{-7}m^2/s$)	2.03
Specific heat (kJ/kg K)	1.5
Bulk density(kg·m-3)	741.33±9.33
Porosity (%)	11.9±3.78
Sphericity (%)	64.4±0.020
Diameter (m)	0.009±0.001
Viscous resistance (1·m-2)	35.282
Inertial resistance (1·m-1)	0.333

Table 3.3 Design conditions and assumptions

Items	Condition or assumption
Location	Limmu (latitude 8.06°N ; longitude 36.57°E)
Incident solar radiation, I(W/m^2)	500-700
sunshine hours,td (hr)	9
Wind speed,(m/s)	2.1
Crop	Coffee
Ambient air temperature, Tam (^0C)	27
Maximum allowable temperature, Tmax (^0C)	60
Initial moisture content (%)	55
Final moisture content (%)	11
Ambient relative humidity, Rham (%)	60
Collector efficiency, η (%)	72
The distance between two adjacent trays (m)	140 mm
loading rate (m_p) kg	50

3.3 Proposed Design

The collector includes a frame of rectangular cross-section having an inlet and outlet for passage of air, a sheet of glass cover at the top of the frame, an absorber plate mounted in the frame below the cover. The absorber is a V-corrugated plate coated with black painted and a jet plate spaced a distance below the absorber plate. Therefore, the jets of air are directed through the inline holes of the jet plate and impinge on the lower surface of the corrugated absorber plate to produce an efficient cooling effect on the absorber plate and leads to improved heat transfer to the flowing air. DC brushless 12V fan of 80 mm diameter is used to propel the air through the solar air heating collector. 30W, 12V solar photovoltaic module is used as a power source to run the fan. The design parameters considered in the analysis will be the jet plate hole diameter, the spacing of the jet plate below the absorber plate and jet-to-jet spacing and distribution of heated air in the drying chamber. Uniform airflow distribution in the drying chamber is very important because it gave a significant effect on the efficiency and the homogeneity of the product being dried. Design optimization of a drying chamber is necessary to achieve higher heat and mass transfer rates and uniform drying by avoiding an unfavorable aerodynamic phenomenon in the chamber.

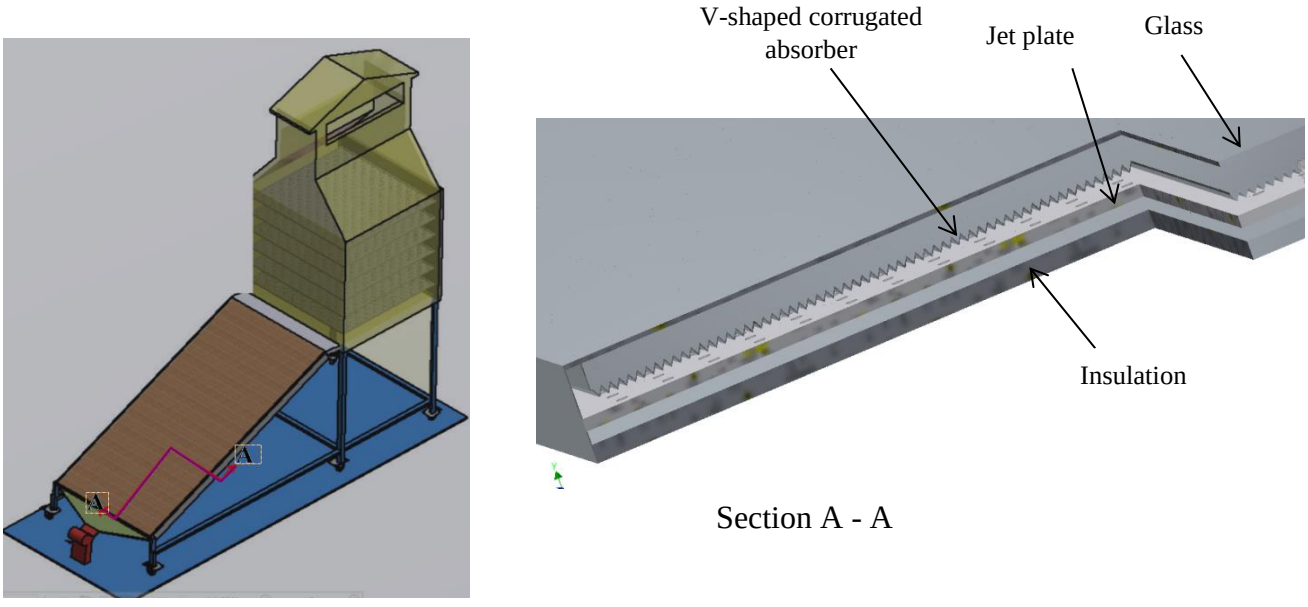

Figure 3. 5 Propose design of the solar coffee dryer

CHAPTER FOUR

4 Design Solar Collector and Drying Chamber

The model designed and simulated for the study of various flow parameters in the solar collector and drying chamber separately due to the limation of the capacity of computer processing and geometry complexity. Therefore the output of collector is used as an input to the drying chamber.

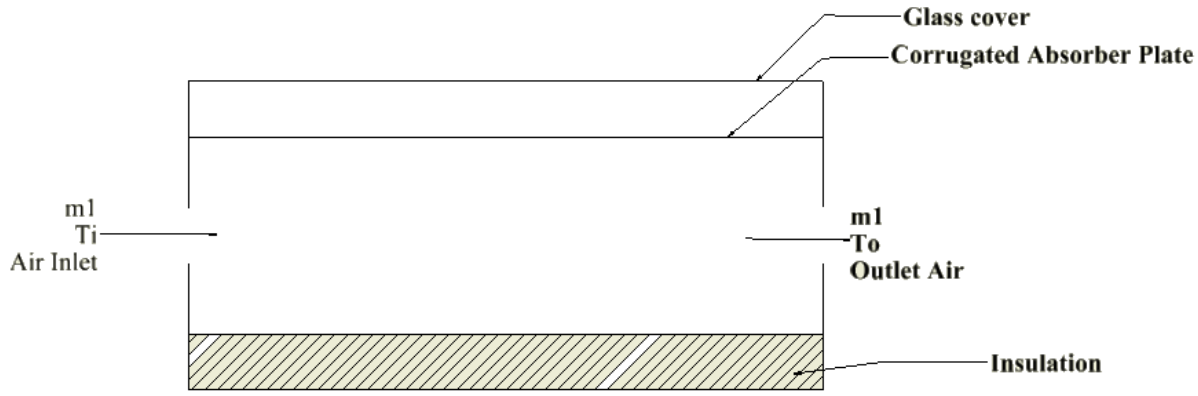

Figure 4. 1 cross-sectional view of conventional parallel flow solar collector

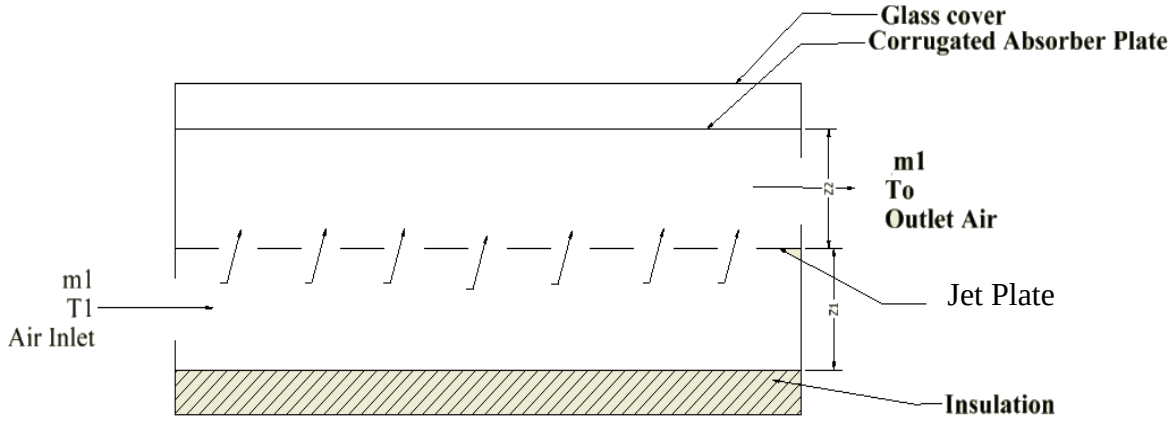

Figure 4. 2 cross-sectional view of cross-flow jet plate solar air heater

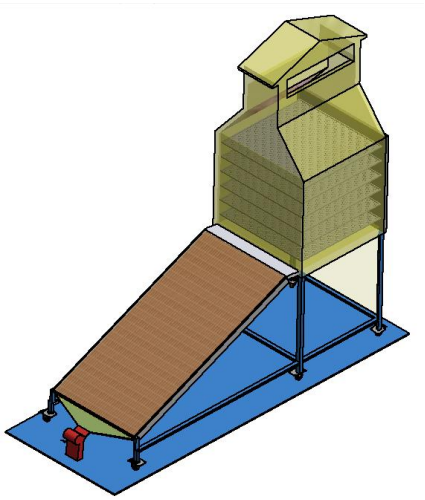

Figure 4. 3 A Solar collector with the drying chamber

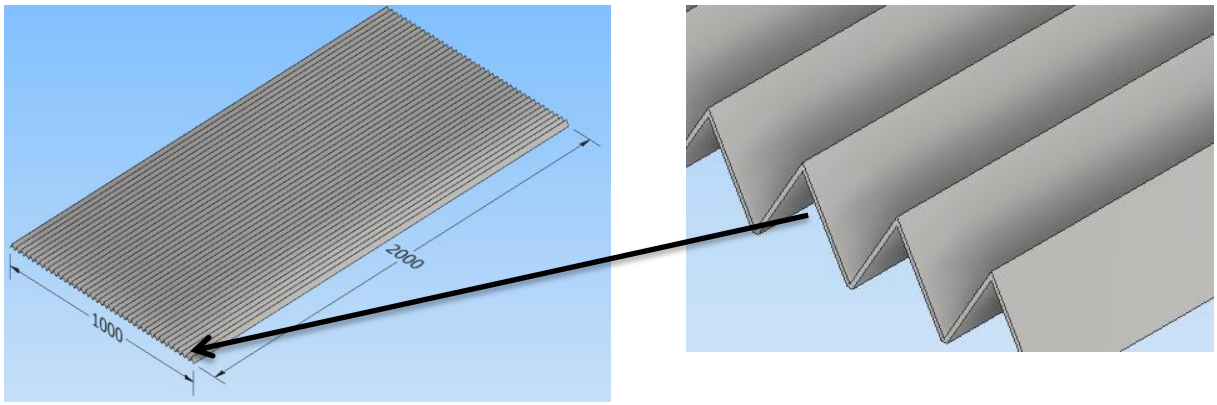

Figure 4. 4 Absorber Plate

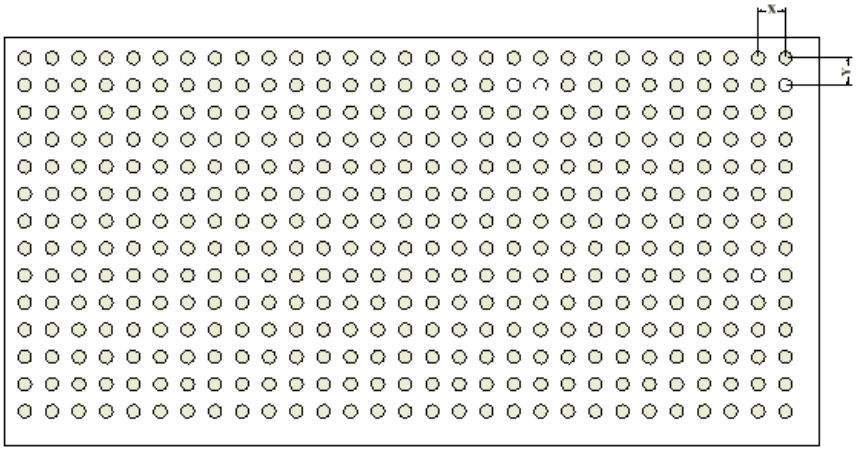

Figure 4. 5 **Jet plate with an inline configuration.**

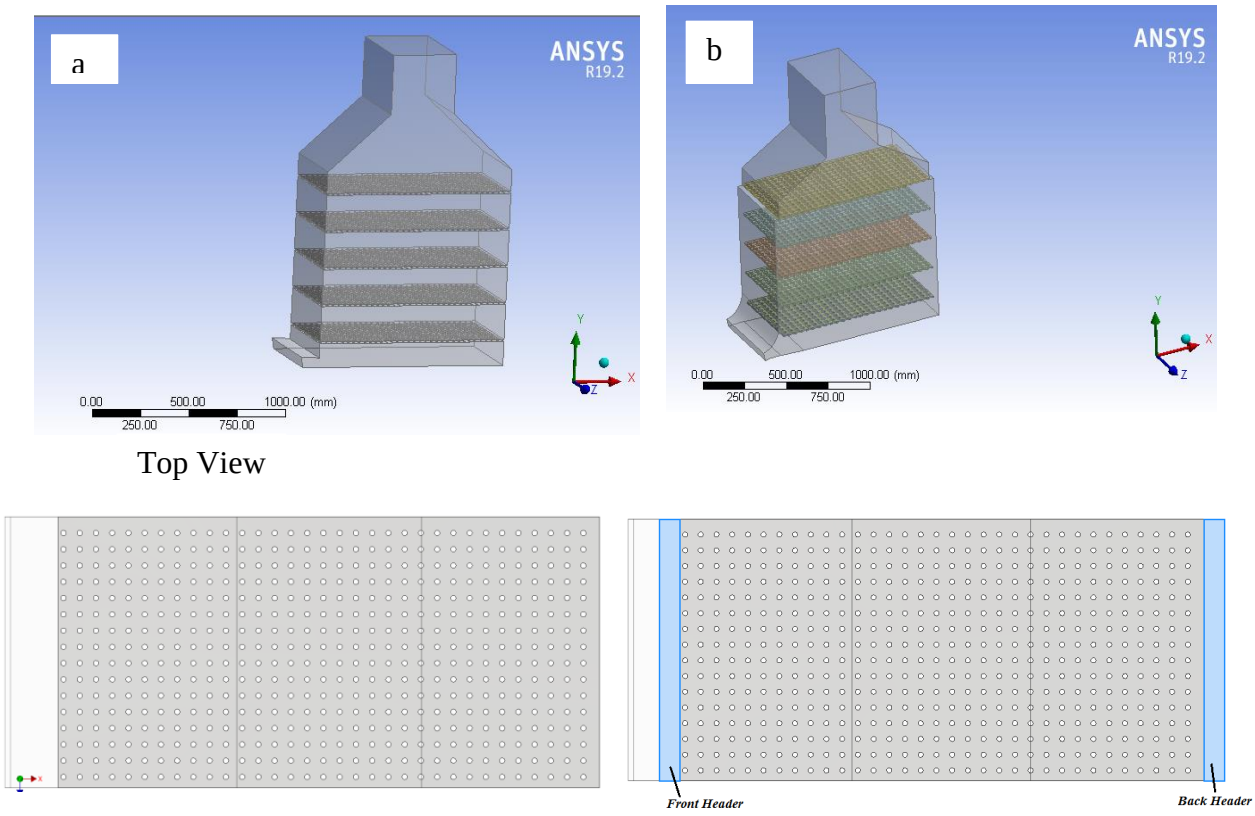

Figure 4. 6 **Drying chamber without (a) and with a header at the front and back side (b)**

Table 4.1 Operating and Design parameters used in the study

1	Length of the solar air heater	L = 2.0 m
2	Width of collector	W = 1.0 m
3	Jet diameters	6,8,10 mm
4	Stream and Spanwise pitch [X, Y]	15mm
5	Jet-to-absorber plate spacing [Z_1]	30 mm
6	The spacing between the bottom and a jet plate[Z_2]	30 mm
7	Absorber plate	t = 1.0 mm, ε_p= 0.95
8	Jet plate	t = 4.0 mm, material: Al – alloy
9	Glass cover	t = 4.0 mm, ε_g = 0.88
10	Absorber Plate-to-cover spacing	20 mm
11	Insulation thickness	t = 20 mm

12	Drying chamber	Length=1m, height=1.5, width=1 m
13	Number of trays	5
14	Tray Thickness	10 mm
15	The distance between the two trays	140 mm
16	Mass flow rate	$\dot{m}1$= 0.02-0.05 kg/s
17	Tilt angle	$\theta = 18.06^0$
18	Solar radiation intensity	500-800 W/m^2
19	Wind velocity	2.1 m/s
20	Ambient temperature	300 K

4.1 Mathematical Modeling of solar collector

4.1.1 Energy balance Equations

The solar radiation absorbed by the absorbing plate per unit area S (W/m^2), which is equal to the difference between the incident solar radiation and the optical loss, is obtained as [1]. To model the collector a number of simplifying assumptions can be made. These assumptions are as follows:

- ✓ Thermal performance of collector is steady state.
- ✓ There is a negligible temperature drop through the glass cover, the absorbing plate, and the bottom plate.
- ✓ There is one-dimensional heat flow through the back insulation, which is in the direction perpendicular to the air flow.
- ✓ Side losses are neglected.
- ✓ The mean temperatures of jet plate, and bottom plate are *T*j and *T*b, respectively, and their variations are neglected.
- ✓ The inlet air temperature approximately equal to the surrounding air temperature and also with the same temperature the air strikes the bottom plate; therefore (Tf1 = Ta = Tb).
- ✓ Mean plate temperature (Tap)=105^0C

The energy balance equations and thermal circuit diagram for the cover, absorber, jet plate, back plate, the air in the passage between the back plate and jet plate and air in the passage between absorber and back plate are represented as follow.

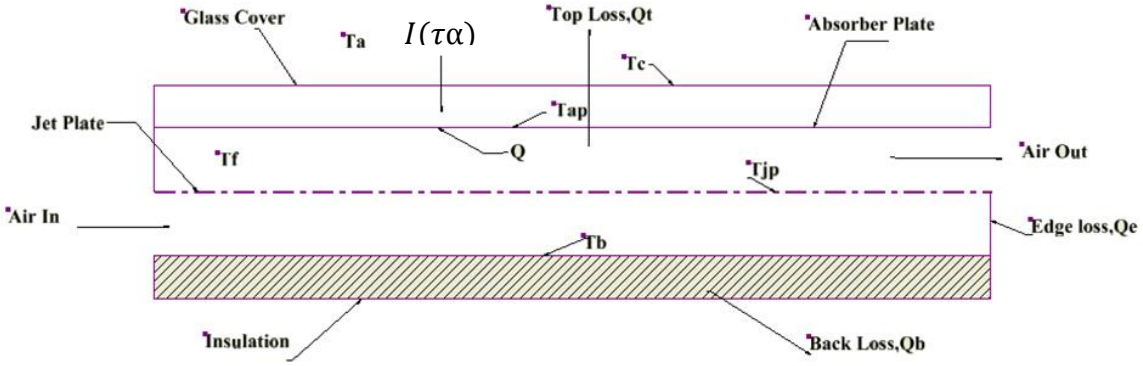

Figure 4. 7 Longitudinal section of the solar air heater with plane view

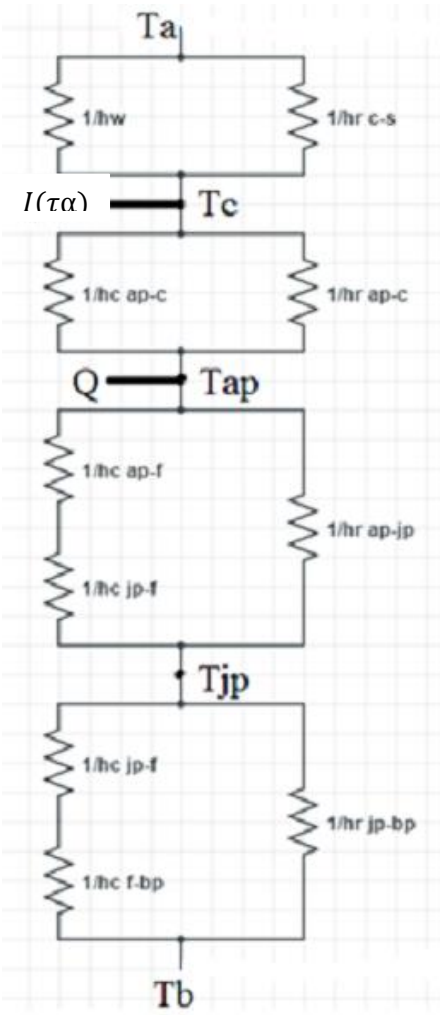

Figure 4. 8 Thermal resistance network for the single cover solar air collector

Solar radiations received by the collector can be expressed by the following equation

$$Q_i \cong \tau_c \alpha_{ap} I \tag{4.1}$$

For glass cover

The absorptivity of solar radiation by the glass cover is α_c, so the energy gain is αcI. Hence, the energy balance for the glass cover requires

$$\alpha_c I + (h_{cap-c} + h_{rap-c})(T_{ap} - T_c) = (h_w + h_{rc-s})(T_c - T_a) \tag{4.2}$$

For the absorber plate

The absorbed solar radiation (S) is distributed to thermal losses to the glass cover by natural convection represented by hc, ap–c and by thermal radiation represented by hr, ap–c, to the jet plate by thermal radiation represented by hr, ap–j, which is the radiation heat transfer coefficient between the absorbing plate and the jet plate, and to the fluid by convection represented by hc, ap–a2 (W/m^2 K), which is the convection heat transfer coefficient of the fluid on the absorbing plate.

$$\alpha_p \tau_g I = h_{c,p-c}(T_p - T_c) + h_{r,p-c}(T_p - T_c) + h_{c,p-a2}(T_p - T_{a2}) + h_{r,p-j}(T_p - T_j) \tag{4.3}$$

For air flow at a lower channel above the jet plate

$$h_{c,p-a2}(T_p - T_{a2}) = q_{u2} + h_{c,j-a2}(T_{a2} - T_j) \tag{4.4}$$

For jet plate

$$h_{r,p-j}(T_p - T_j) + h_{c,j-a2}(T_{a2} - T_j) = h_{c,j-a1}(T_j - T_{a1}) + h_{r,j-bp}(T_j - T_{bp}) \tag{4.5}$$

For air at a lower channel below the jet plate

$$q_{u1} = h_{c,j-a1}(T_j - T_{a1}) + h_{c,bp-a1}(T_{bp} - T_{a1}) \tag{4.6}$$

For backplate

$$h_{r,j-bp}(T_j - T_{bp}) = h_{c,bp-a1}(T_{bp} - T_{a1}) + U_b(T_b - T_a) \tag{4.7}$$

4.4.2 Heat transfer coefficients

Convective heat transfer coefficient (*hw*) for ambient air flowing over the outside surface of the glass cover depends primarily on the wind velocity. It is taken from [36] and given by

$$h_w = \begin{Bmatrix} 5.7 + 3.8V_w ....V_w \le 5m/s \\ 6.5V_w^{0.8} .....V_w \ge 5m/s \end{Bmatrix} \quad (4.8)$$

Therefore for the selected site V_w= 9.3 km/h or 2.1 m/s [36]

h_w= 5.7 + 3.8 V_w=13.6 W/m^2K

Iteration 1

The procedure is to estimate the cover temperature, from which *hc,ap−c*, *hr,ap−c* and *hr,c−s* are calculated. With these heat transfer coefficients and *hw*, the top loss coefficient is calculated. These results are then used to calculate *Tc* from the preceding equation. If *Tc* is close to the initial guess, no further calculations are necessary. Otherwise, the newly calculated *Tc* is used and the process is repeated.

Assume initial guess for mean cover plate temperature *T*c =35^{0}C. In order to calculate the convective heat transfer coefficient between the absorber and the cover, the air properties will be considered at mean temperature between the absorber and the glass cover, i.e. 70^{0}C. Air properties at 70^{0}C and 1 atm are obtained from table. [37].

$\rho = 1.028$ kg/m^3
$k = 0.02881$ W/m.°C
$\nu = 1.995\times10^{-5}$ m^2/s

$c_p = 1007$ J/kg.°C
Pr = 0.717
μ=2.052×10^{-5} kgm/s

The Rayleigh number is:

$$Ra = Gr\,\Pr = \frac{g\beta'\Delta TH_c^{\ 3}}{\nu^2} = \frac{9.81x(105-35)(0.02)^3 x0.717}{343x(1.995x10^{-5})^2} = 28861.327 \quad (4.9)$$

In which ρ (kg/m^3), β (1/K) and μ (kg/m s) are the density, thermal- expansion coefficient and dynamic viscosity of air, and g (m/s^2) is the acceleration due to gravity.

Nusselt number is the ratio of the convective heat transfer to the conductive heat transfer.

Nu can be obtained from the expression

$$Nu = 1 + 1.44\left[1 - \frac{1708}{Ra\cos\theta}\right]^{+}\left(1 - \frac{1708\sin(1.8\theta)^{1.6}}{Ra\cos\theta}\right) + \left[\left\{\frac{Ra\cos\theta}{5830}\right\}^{1/3} - 1\right]^{+} \quad (4.10)$$

"+" exponent means only the positive value of the term in square bracket is to be considered, Zero is to be used for negative values, and the angle of inclination can vary between 0 – 75^{O},

$$Nu = 3.008$$

The convective heat transfer coefficient is, therefore

$$h_{c\ ap-c} = Nu\frac{k}{Hc} = 3.008\frac{0.02881}{0.02} = 4.3333W/m^2.^oC \quad (4.11)$$

The radiative heat transfer coefficient from the glass cover to the sky can be calculated by using the formula given by

$$h_{r,c-a} = \frac{\varepsilon_g\sigma[(T_c+273)^4 - (T_{sky}+273)^4]}{T_c - T_a} = 17.24W/m^2.^0C \quad (4.12)$$

where $\sigma=5.67\times10^{-8}$ W/m^2 K^4 is the Stefan–Boltzmann constant, Ts is the sky temperature and it is given by [38]

$$T_S = 0.0552\ Ta^{1.5} = 7.74^oC \quad (4.13)$$

The radiative heat transfer coefficients between the glass cover and absorber plate are calculated using the following relation

$$h_{r,ap-c} = \frac{\varepsilon_{ff}\sigma[(T_{ap}+273)^4 - (T_c+273)^4]}{T_{ap} - T_c} = 7.7679W/m^2.^0C \quad (4.14)$$

$$U_t = \left\{\frac{1}{h_{c,ap-c}+h_{r,ap-c}} + \frac{1}{h_w + h_{r,c-a}}\right\}^{-1} = 8.6907W/m^2.^0C$$

The cover temperature is

$$T_c = T_{ap} - \frac{U_t(T_{ap}-T_a)}{h_{c,ap-c}+h_{r,ap-c}} = 48.98^oC$$

Iteration 2

Air properties at mean temperature of Tap and the new Tc=49^{0}C, atTm ≈77^{O}C are:

$\rho = 1.028$ kg/m^3

$k = 0.03$ W/m.°C

$T = 350K$

$\nu = 2.076\times10^{-5}$ m^2/s

$c_p = 1007$ J/kg.°C

$\Pr = 0.697$

$\mu = 2.052\times10^{-5}$ kgm/s

$$Ra = Gr\,\Pr = \frac{g\beta'\Delta T H_c^{\,3}}{\nu^2} = \frac{9.81x(105-49)(0.02)^3 x0.697}{350x(2.076x10^{-5})^2} = 20286.105 \qquad (4.15)$$

The Nusselt number is 2.75, with this new estimate of the cover temperature, the various heat transfer coefficients become;

$$h_{c\ ap-c} = Nu\frac{k}{Hc} = 2.75\frac{0.02881}{0.02} = 3.965W/m^2.^oC \qquad (4.16)$$

$$h_{r,c-a} = \frac{\varepsilon_g\sigma[(T_c+273)^4-(T_{sky}+273)^4]}{T_c-T_a} = 10.24W/m^2.^0C$$

$h_{r,ap-c} = \dfrac{\varepsilon_{ff}\sigma[(T_{ap}+273)^4-(T_c+273)^4]}{T_{ap}-T_c} = 8.22W/m^2.^0C$ and the second estimate of Ut is

$$U_t = \left\{\frac{1}{h_{c,ap-c}+h_{r,ap-c}} + \frac{1}{h_w+h_{r,c-a}}\right\}^{-1} = 8.0634W/m^2.^0C \qquad (4.17)$$

$$T_c = T_{ap} - \frac{U_t(T_{ap}-T_a)}{h_{c,ap-c}+h_{r,ap-c}} = 53.38^oC \qquad (4.18)$$

Iteration 3

Air properties at mean temperature of Tap and the new Tc=53.38^{0}C, at ≈79.19^{O}C are:

$\rho = 1.028\ \text{kg/m}^3$

$k = 0.02947\ \text{W/m.°C}$

$T = 352.2K$

$\nu = 2.097\times10^{-5}\ \text{m}^2/\text{s}$

$c_p = 1007\ \text{J/kg.°C}$

$\text{Pr} = 0.7154$

$\mu = 2.096\times10^{-5}\ \text{kgm/s}$

$$Ra = Gr\,\text{Pr} = \frac{g\beta'\Delta TH_c^{\ 3}}{\nu^2} = \frac{9.81x(105-53.38)(0.02)^3 x0.7154}{352.2x(2.097x10^{-5})^2} = 18724.57$$

Similarly the Nusselt number is 2.698, with this new estimate of the cover temperature, the various heat transfer coefficients become;

$$h_{c\ ap-c} = Nu\frac{k}{Hc} = 2.6975\frac{0.02953}{0.02} = 3.983W/m^2.^oC$$

$$h_{r,c-a} = \frac{\varepsilon_g\sigma[(T_c+273)^4-(T_{sky}+273)^4]}{T_c-T_a} = 9.67W/m^2.^0C$$

$h_{r,ap-c} = \dfrac{\varepsilon_{ff}\sigma[(T_{ap}+273)^4-(T_c+273)^4]}{T_{ap}-T_c} = 8.367W/m^2.^0C$ and the third estimate of Ut is

$$U_t = \left\{\frac{1}{h_{c,ap-c}+h_{r,ap-c}} + \frac{1}{h_w+h_{r,c-a}}\right\}^{-1} = 8.06817W/m^2.^0C$$

$$T_c = T_{ap} - \frac{U_t(T_{ap}-T_a)}{h_{c,ap-c}+h_{r,ap-c}} = 54.04^oC$$

Iteration 4

Air properties at mean temperature of Tap and the new Tc=54.04^{0}C, at Tm≈79.52^{O}C are:

$\rho = 1.001\ \text{kg/m}^3$

$k = 0.02949\ \text{W/m.°C}$

$T = 352.52K$

$\nu = 2.092\times10^{-5}\ \text{m}^2/\text{s}$

$c_p = 1008$ J/kg.°C

$\Pr = 0.7158$

$\mu = 2.094 \times 10^{-5}$ kgm/s

$$Ra = Gr \Pr = \frac{g\beta' \Delta T H_c^{\ 3}}{\nu^2} = \frac{9.81x(105-54.04)(0.02)^3 x0.7158}{352.52x(2.092x10^{-5})^2} = 18537.83$$

Similarly the Nusselt number is 2.6906, with this new estimate of the cover temperature, the various heat transfer coefficients become;

$$h_{c\ ap-c} = Nu\frac{k}{Hc} = 2.6906\frac{0.02949}{0.02} = 3.97W/m^2.^oC$$

$$h_{r,c-a} = \frac{\varepsilon_g \sigma[(T_c+273)^4 - (T_{sky}+273)^4]}{T_c - T_a} = 9.604W/m^2.^0C$$

$$h_{r,ap-c} = \frac{\varepsilon_{ff} \sigma[(T_{ap}+273)^4 - (T_c+273)^4]}{T_{ap} - T_c} = 8.389W/m^2.^0C$$ and the forth estimate of *Ut* is

$$U_t = \left\{ \frac{1}{h_{c,ap-c} + h_{r,ap-c}} + \frac{1}{h_w + h_{r,c-a}} \right\}^{-1} = 8.064W/m^2.^0C$$

$$T_c = T_{ap} - \frac{U_t(T_{ap} - T_a)}{h_{c,ap-c} + h_{r,ap-c}} = 54.10^oC$$

Iteration 5

Air properties at mean temperature of Tap and the new Tc=54.10^{0}C, at Tm≈79.55^{O}C are:

$\rho = 1.001$ kg/m^3

$k = 0.02949$ W/m.°C

$T = 352.52K$

$\nu = 2.092 \times 10^{-5}$ m^2/s

$c_p = 1008$ J/kg.°C

$\Pr = 0.7158$

$\mu = 2.094 \times 10^{-5}$ kgm/s

$$Ra = Gr\,\Pr = \frac{g\beta'\Delta TH_c^{\,3}}{\nu^2} = \frac{9.81x(105-54.04)(0.02)^3 x0.7158}{352.55x(2.092x10^{-5})^2} = 18537.83$$

Similarly the Nusselt number is 2.6906, with this new estimate of the cover temperature, the various heat transfer coefficients become;

$$h_{c\ ap-c} = Nu\frac{k}{Hc} = 2.6906\frac{0.02949}{0.02} = 3.97W/m^2.^oC$$

$$h_{r,c-a} = \frac{\varepsilon_g\sigma[(T_c+273)^4-(T_{sky}+273)^4]}{T_c-T_a} = 9.604W/m^2.^0C$$

$$h_{r,ap-c} = \frac{\varepsilon_{ff}\sigma[(T_{ap}+273)^4-(T_c+273)^4]}{T_{ap}-T_c} = 8.389W/m^2.^0C$$

and the forth estimate of *Ut* is

$$U_t = \left\{\frac{1}{h_{c,ap-c}+h_{r,ap-c}} + \frac{1}{h_w+h_{r,c-a}}\right\}^{-1} = 8.064W/m^2.^0C$$

$$T_c = T_{ap} - \frac{U_t(T_{ap}-T_a)}{h_{c,ap-c}+h_{r,ap-c}} = 54.11^oC$$

The radiative heat transfer coefficients between the absorber plate and jet plate is calculated using the following relation

$$h_{r,p-j} = \frac{\sigma(T_p^{\,2}+T_j^{\,2})(T_p-T_j)}{\frac{1}{\varepsilon_p}+\frac{1}{\varepsilon_j}-1} \qquad (4.15)$$

The radiative heat transfer coefficients between the jet plate and the back plate is calculated using the following relation

$$h_{r,j-bp} = \frac{\sigma(T_j^{\,2}+T_{bp}^{\,2})(T_j-T_{bp})}{\frac{1}{\varepsilon_j}+\frac{1}{\varepsilon_{bp}}-1} \qquad (4.16)$$

4.1.3 Energy Loss Coefficients

The collector overall energy loss coefficient, U_L takes into account top, bottom and edge heat losses and can be written as [39] .

$$U_L = U_t + U_b + Ue \tag{4.19}$$

Back insulation is wood wool with insulation conductivity of K = 0.045 /W m K and 20 mm thickness of insulation.

$$U_b = \frac{k_{in}}{\delta_{in}} = \frac{0.045}{0.02} = 2.25W/m^2k \tag{4.20}$$

Edge Loss Coefficient

$$U_e = U_b \frac{Ae}{Ac} \tag{4.21}$$

$$Ae = 2(2*1)0.003 = 0.012m^2$$

$$U_e = U_b \frac{Ae}{Ac} = 0.013W/m^2k$$

Therefore $U_L = U_t + U_b + Ue = 10.327W/m^2k$

The overall heat lost by the absorber to the ambient per unit area is expressed as

$$\dot{q} = U_L(T_c - T_a) = 10.32W/m^{2o}C(54.10-27)^0C = 275.96W/m^2$$

Useful energy gain by solar air heater is calculated as

$$Q_u = Q_i - Q_l = 576 - 275.96 = 300.04W/m^2$$
$$Q_u = 600.08W \tag{4.22}$$

The collector heat removal factor F_R is calculated as

Assume collector efficiency factor (F$^{'}$) of 0.8

$$F_R = \frac{mC_p}{U_L Ac}\left[1 - e^{\left(\frac{-AcU_L F'}{mC_p}\right)}\right] = 0.73 \tag{4.23}$$

$$Q_u = F_R Ac(\tau\alpha I - U_L(T_o - T_i)) = 600.08W$$

From this outlet temperature will be

$$T_o = T_i + \frac{\left[\tau\alpha I - \frac{Q_u}{F_R Ac}\right]}{U_L} = 333K \quad (4.24)$$

$$Q_u = hA(T_0 - T_i) = 600.08W$$

$$h = \frac{600.08W}{2m^2(333k - 300k)} = 9.09W/m^2k \quad (4.25)$$

With the help of *To*, thermal efficiency is calculated as

$$\eta_{th} = \frac{mCp(T_o - T_i)}{AcI} = \frac{0.024x1007(333-300)}{2x600} = 0.6646 \quad (4.26)$$

$$Dh = \frac{WH_g}{1+0.5H_g} = \frac{1*0.06}{1+0.05(0.06)} = 0.582m \quad (4.27)$$

Cross sectional area of upper and lower channel,

$A_2 = WZ_2 = 1*0.03 = 0.03m^2$,

The Reynolds number is [33]

$$Re = \frac{\rho VDh}{\mu} = \frac{mDh}{A_f\mu} = \frac{0.024(0.582)}{1x0.06x1.9498x10^{-5}} = 12437.17 \quad (4.28)$$

Where *V* is the bulk velocity in the stream-wise direction, *D*h is the hydraulic diameter of the channel, and *v* is the kinematic viscosity of air.

Therefore, assume fully developed turbulent flow in the entire duct, and determine the Nusselt number from [40]

$$Nu = \frac{hD_h}{k} = 0.023\,\mathrm{Re}^{0.8}\,\mathrm{Pr}^{0.3} = 0.023(12437.17)^{0.8}(0.72357)^{0.3} \quad (4.29)$$

$$Nu = 39.38$$

The friction factor is Friction factor (f) is the parameter used to calculate the frictional resistance of the fluid passing through the channel and it is defined as [37]. Friction factor in the upper channel of cross flow jet plate solar air heater with inline holes,

The friction factor, the pressure drop, and then the fan power can be determined for the case of fully developed turbulent flow to be

$$f = 0.184\,\mathrm{Re}^{-0.2} = 0.184(12437.17)^{-0.2} = 0.0279$$

$$f = \frac{\Delta p D_2}{2\rho L V_2} \tag{4.30}$$

Where, pressure drop in the flow channel,

$$\Delta P = f\,\frac{L}{D}\,\frac{\rho V_{avg}^2}{2} = 0.0279\,\frac{(2\text{ m})}{(0.582\text{ m})}\,\frac{(1.1022\text{ kg/m}^3)(\,3\text{m/s})^2}{2} = 1.656\text{ N/m}^2 \tag{4.31}$$

Table 1.2 Results under the typical configurations and operating conditions.

No.	Parameters	Value (unit)
1.	Solar radiations received by the collector	576W/m^2
2.	Useful energy gain by solar air heater	600.08W
3.	Top loss coefficient (Ut)	8.064 W/m^2 .^oC
4.	Bottom loss coefficient (Ub)	2.25 W/m^2 .k
5.	Edge loss coefficient (Ue)	0.013 W/m^2 .k
6.	Overall heat transfer coefficient (h_L)	9.09 W/m^2 .k
7.	Collector efficiency factor ($F^{'}$)	0.8
8.	Heat removal factor (FR)	0.73
9.	Thermal efficiency of collector	66.46 %

4.2 Mathematical Modeling of Solar Dryer

A solar coffee dryer transforms solar energy into heat that helps diminish the humidity of the coffee grains; the quantity of water that can be reduced by evaporation from the coffee grains depends mainly on the air temperature and velocity of air circulation in drying chamber.

4.2.1 Factors Affecting the Rate of Drying

Drying Temperature

Temperature has a direct effect on the rate of drying and hence is considered to be one of the key factors for consideration in any drying system. In coffee drying, it is the temperature of the coffee, not of the drying air, that is of importance in the drying process. The recommended range for coffee drying temperatures is 30°C to 60 °C.[41]

Relative Humidity

Relative humidity is the ratio of the partial pressure of the water vapor to the equilibrium vapor pressure of water at the same temperature. The relative humidity of air is an indicator of the drying capacity of the air. A low value of RH is generally an indication of high drying capacity.

Velocity of Air

In general, for high moisture content coffee, as the air velocity increases, the drying rate increases and is more uniform. Therefore, at the initial phase of drying, high velocity of drying air will ensure a faster rate of moisture removal from the wet parchment coffee.

Air Drying Potential

The drying potential of air is defined as the drying force that accomplishes drying and is measured by the difference between the water vapor pressure of the material to be dried and that of the drying air. The excess of the material vapor pressure over that of air constitutes the drying potential and influence the rate of drying. When the material vapor pressure equals that of the drying air, the drying potential becomes zero and drying ceases. [41]

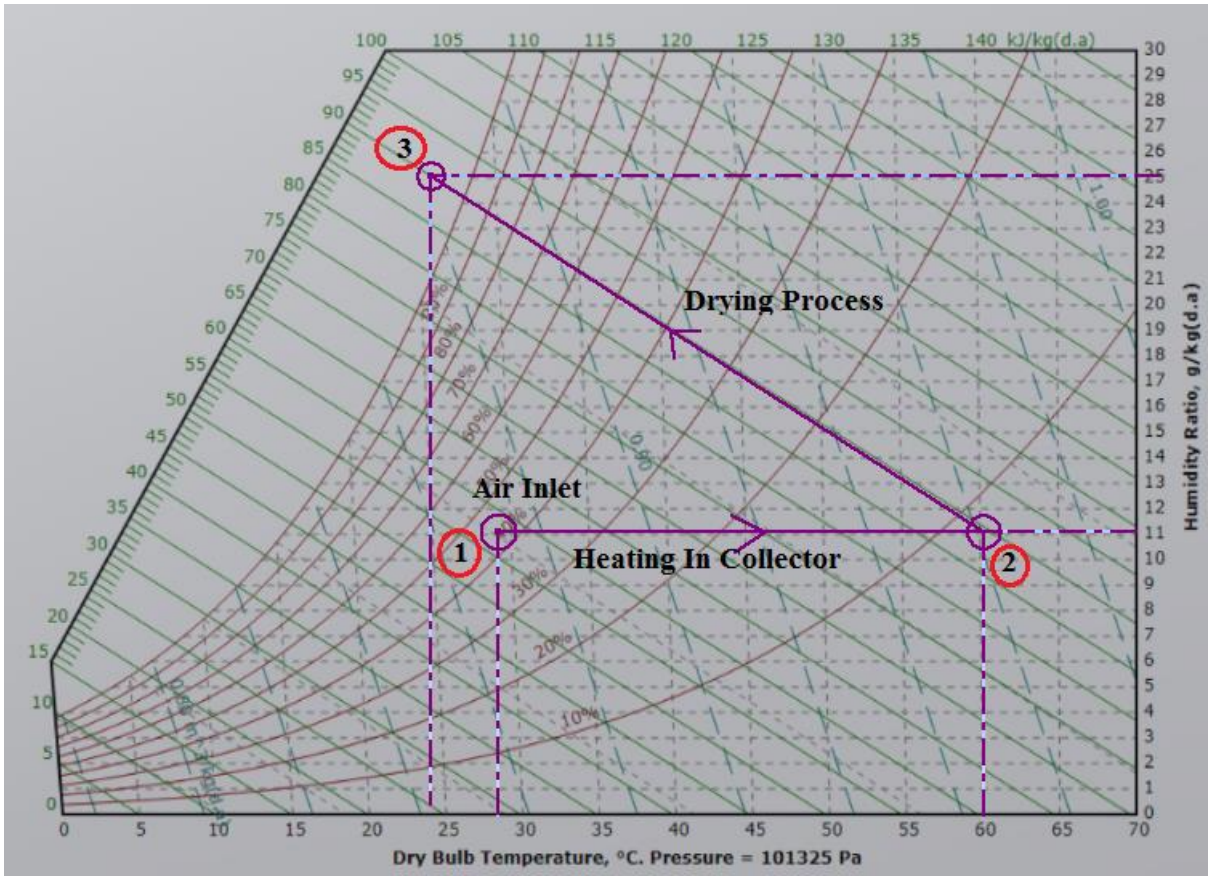

Figure 4. 10 Drying Process on Psychometric Chart [42]

Table 4.3 Psychometric property of air at evaluation conditions

At point 1			
Dry bulb temperature,	**T =**	**27.00**	**^{o}C**
Relative humidity,	**RH=**	**50.00**	**%**
Wet bulb temperature,	T_w=	19.60	^{o}C
Dew-point temperature,	T_{dp}=	15.60	^{o}C
Humidity at T,	W =	0.0111	kg water/kg dry air
Saturation humidity at T,	W_s=	0.023	kg water/kg dry air
Saturation humidity at T_w,	W_w=	0.014	kg water/kg dry air
Percentage saturation,	PS=	49.1%	
Enthalpy,	hi =	55.6	kJ/kg dry air
Humid volume,	v_H=	0.864	m^3/kg dry air
Humid heat,	c_s=	1.026	kJ/kg dry air ^{o}C
Density of humid air,	ρ =	1.170	kg/m^3
Partial pressure of water vapor in the air	p =	1783.3	Pa
At point 2			
Dry bulb temperature,	**T =**	**60.00**	**^{o}C**
Humidity at T,	**W =**	**0.0111**	**kg water/kg dry air**
Wet bulb temperature,	T_w=	28.20	^{o}C
Dew-point temperature,	T_{dp}=	15.40	^{o}C
Saturation humidity at T,	W_s=	0.152	kg water/kg dry air
Saturation humidity at T_w,	W_w=	0.025	kg water/kg dry air
Relative humidity,	RH=	8.91%	
Percentage saturation,	PS=	7.3%	
Enthalpy,	hf =	89.3	kJ/kg dry air
Humid volume,	v_H=	0.959	m^3/kg dry air
Humid heat,	c_s=	1.026	kJ/kg dry air ^{o}C
Density of humid air,	ρ =	1.054	kg/m^3
Partial pressure of water vapor in the air	p =	1776.5	Pa

4.2.2 Determination of the Various Drying Parameters

Moisture of coffee is evaporated into drying air without any heat input or removal (this is the meaning of the term *'adiabatic'*), the latent heat of evaporation is taken from the atmosphere. The sensible heat content - thus the DBT - is reduced, but the latent heat content is increased. The status point moves up and to the left, along a WBT line. This is the process the relative humidity is increased and involved in evaporative cooling.

a) The quantity of heat required to evaporate the water would be;

$$Q = m_w h_{fg} \tag{4.31}$$

Where Q=the amount of energy required for the drying process, kJ

m_w =mass of water, kg

h_{fg}=latent heat of evaporation, kJ/kg

b) Amount of water to be removed;

$$m_w = m_p \frac{m_i - m_f}{100 - m_f} \tag{4.32}$$

Where, *mi*=initial moisture content, % wet basis;

mf=final moisture content, % wet basis;

mw=Amount of water to be removed of water, kg;

mp=initial mass of product to be dried, kg.

$$m_w = 50\frac{55-11}{100-11} = 24.71kg$$

The amount needed is a function of temperature and moisture content of the crop. The latent heat of vaporization is calculated as follows [41]

$$h_{fg} = 4.186x103(597 - 0.56T_m) = 2.429x10^5\ J/kg$$

Where: Tm -maximum allowable temperature (60^{o}c)

Where, hfg = specific latent heat of vaporization of water from the coffee beans surface (J/kg).

The total heat energy, E (kJ) required to evaporate water was calculated as follows [43]

$$E = \dot{m}(h_f - h_i)t_d = \frac{A_c I\eta}{10000} = 8.18kJ \quad (4.34)$$

Where: E = total heat energy, kJ m` = mass flow rate of air, kg/hr hf and hi = final and initial enthalpy of drying and ambient air, respectively, kJ/kg dry air. td = drying time, hrs

The enthalpy of moist air in J/kg at temperature T(◦C) can be approximated [43].

$$h = 1006.9T + m_w(251213.0 + 1552.4T) \quad (4.35)$$

c) The quantity of air needed for drying

Using Psychometric property of air and taking input air temperature of 27°C (dry bulb) and a relative humidity of 50%, the psychometric chart gives a humidity ratio of 0.011 kg water/kg dry air. When the solar collector heats air to drying temperature of 60°C (dry bulb), the humidity ratio remains constant. If on passing through the coffee, the air absorbs moisture until its saturation line. The psychometric chart shows the humidity ratio to be 0.025 kg water/kg dry air. The change in humidity ratio is therefore: 0.025 - 0.011 = 0.014 and the corresponding dry bulb temperature is 28.2°C.For a humidity ratio increase of 0.014 kg water/ kg dry air, each kg of water will require 1/0.014 = 71 kg dry air.

From the gas laws equation

$$PV = M_A RT \quad (4.36)$$

Where;

P = is the atmospheric pressure = 101.3 KPa,

V =the volume of air in m^3.

M_A = the mass of the air in kg,

T =the absolute temperature in Kelvin, and

R = the gas constant = 0.291 kPa m³/kg K.

The absolute temperature is 28.2+273 = 301.2K and the volume of air needed to remove 1 kg of water is 61.43 m^3.Hence 24.71 kg will require 1517.9m^3 volume of air.

The volume flow rate of air V_a (m^3/hr)

$$V_a = \frac{W_a}{t_d}$$

W_a = quantity of air required in m^3 = 1358.89m^3

t_d =Total drying time=6 hrs (a batch daily)

V_a= 1517.9/6 =252.99m^3/hr

Mass flow rate of air, m_a, kg/hr

$$m_a = \rho_a \times V_a = 303 kg/hr$$

ρ_a= density of drying air (Kg/m^3)=1.2kg/m^3

V_a= volumetric air flow rate

d) Average drying rate

The drying rate is proportional to the difference in the moisture content between materials to be dried and the equilibrium moisture content. Average drying rate m_{dr} can be determined from the mass of moisture removed by solar heat and drying time (td) by the equation shown below;

Average drying rate m_{dr} was determined from the mass of moisture to be removed by solar heat and drying time by the following equation:

$$m_{dr} = \frac{m_w}{t_d} = \frac{24.71}{6} = 4.12 kg/hr \quad (4.37)$$

e) Final or equilibrium relative humidity

Final relative humidity or equilibrium relative humidity was calculated using sorption isotherms equation for coffee beans as follows

$$aw = 1- \exp[-\exp (0.914+0.5639\ln Mf)] \quad (4.38)$$

Where: aw = water activity, decimal M f= final moisture content dry basis, kg water/kg dry solids

f) Chimney

A chimney is fitted on top of the drying chamber and its main role is to allow moisture ridden-air to escape from the dryer. It minimizes the build-up of moisture above the drying bin which is very undesirable in a drying system and offers the suction effect due to the space created by exhausted air, thus more hot air is forced into the drying chamber.

g) Pressure drop through the drying trays

The resistance to the flow of air through a packed bed of agricultural produce is expressed in [44]

$$u = a(\frac{\Delta P}{h_L}) \quad (4.39)$$

Where; ***u*** is the superficial air velocity,

$\boldsymbol{h_L}$ the drying bed thickness and

a is a constant whose value is determined experimentally.

For forced circulation of air through a thin layer of crop (h_L>0.20 m), the value of the constant is 0.465m^3s/kg.[44]

The air velocity (u) can be assumed as the maximum velocity at the exit of the solar collector [44]. The pressure drop across the coffee (ΔP) is calculated using the optimum drying bed thickness of 0.1 m.

$\Delta P = 1.656 Pa$

The total pressure drop across the solar collector and the air vent is comparable to that across the drying trays, and hence the total pressure drop of the system is twice the pressure drop of the drying trays. Hence, (ΔP_T = 2(ΔP). When all pressure drops are accounted for, experience has shown that the gross pressure drop is about six times the value of ΔP [44].

ΔP_T =6 x (2ΔP) =19.872 Pa (4.40)

4.3 Drying Efficiencies

Ηd is defined as the ratio of the moisture removed or picked-up by the drying air to the theoretical capacity of the air to absorb moisture.

$$\eta_d = \frac{(m_w x h_{fg}) + (M_g x c_{pg} x \Delta T)}{Q_a} \quad (4.41)$$

Where;Qa =MaCpa (Tinto drying chamber – Tambient temperature),

Mw = mass of evaporated water,=24.72 kg

h_{fg}= latent heat of vaporization, = $2.429 x 10^5 J / kg$

Mg = mass of the product dried,=50 kg

Cpg = specific heat capacity of the grains =1500 J/kg K

ΔT = change in temperature of the chamber

$\eta_d = 38.5\%$

Table 4.4 Design parameters and Values for Drying Chamber

Parameter	Values	Equation or data used
Initial humidity ratio, wi, kgH_2O/kg dry air	0.011	Tam, Rham , Psychometric chart
Initial enthalpy,hi, kJ/kg dry air	68.2	Tam, Rham , Psychometric chart
Final enthalpy, hf, kJ/kg dry air	89.3	wi and Tf , Psychometric chart
Equilibrium relative humidity, ERH,%	57	mf and isotherms equation
Final humidity ratio, wf ,kgH_2O/kg dry air	0.025	RHf and hf, , Psychometric chart
Mass of water to be evaporated, mw, kg	24.72	
Latent heat of vaporization J/kg	2.429×10^5	
Average drying rate, mdr, kgH_2O/hr	4.12	
Air flow rate, ma, kg dry air/hr	275.01	
volumetric airflow rate, Va m^3/hr	303	
Total useful energy, E, MJ	58.34	
Solar collector area, Ac,m^2	2	
Dryer Efficiency,%	38.5	

CHAPTER FIVE

5 CFD Investigation

The CFD code ANSYS FLUENT 19.2 carried out the analysis in three main stages as

- ✓ Pre-processing
- ✓ Solver and
- ✓ Post-processing.

5.1 Pre-Processing

This is the first step of the CFD simulation process. In this step initially, modeling goals like the initial assumptions (steady, unsteady, inviscid, laminar, turbulent etc.) applied to a given problem to simplify it, the degree of accuracy needed for computational time etc. After gathering this information, the analysis includes the following main steps:

i) Identify the domain of interest.

ii) Creating a solid model of the domain. The solid model of the domain is generated in Autodesk Inventor Professional software, removing unnecessary features which may complicate meshing or grid generation processes.

5.1.1 Geometry Generation

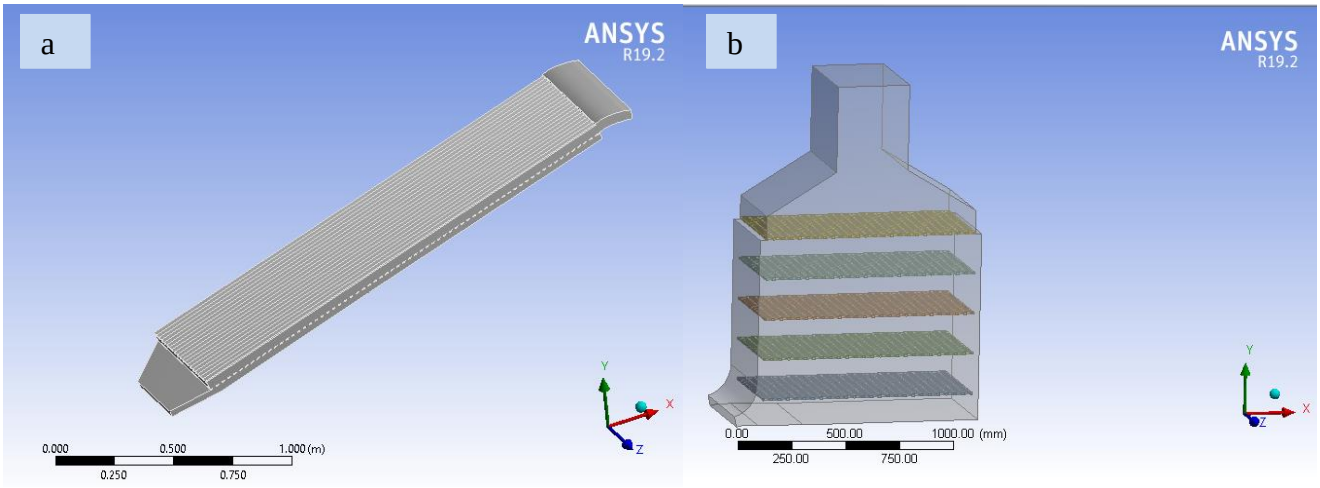

Figure 5. 1 3D Model of Solar Collector (a) and Drying Chamber (b)

5.1.2 Mesh generation

Meshing or grid generation is the most vital part of the CFD analysis. Meshing means dividing the flow domain into a number of subdomains which has a form of geometric primitives like hexahedron and tetrahedron in 3-D and triangles and quadrilaterals in the 2-D physical domain. The subdomains are called an element or cells and collection of all elements or cells is called a mesh or grid. The presence of good meshing has a significant effect on the rate of convergence, solution accuracy and computation time. During meshing, appropriate boundary conditions at cells are specified. The non-uniform grids are generated for all numerical simulations performed in this CFD work.

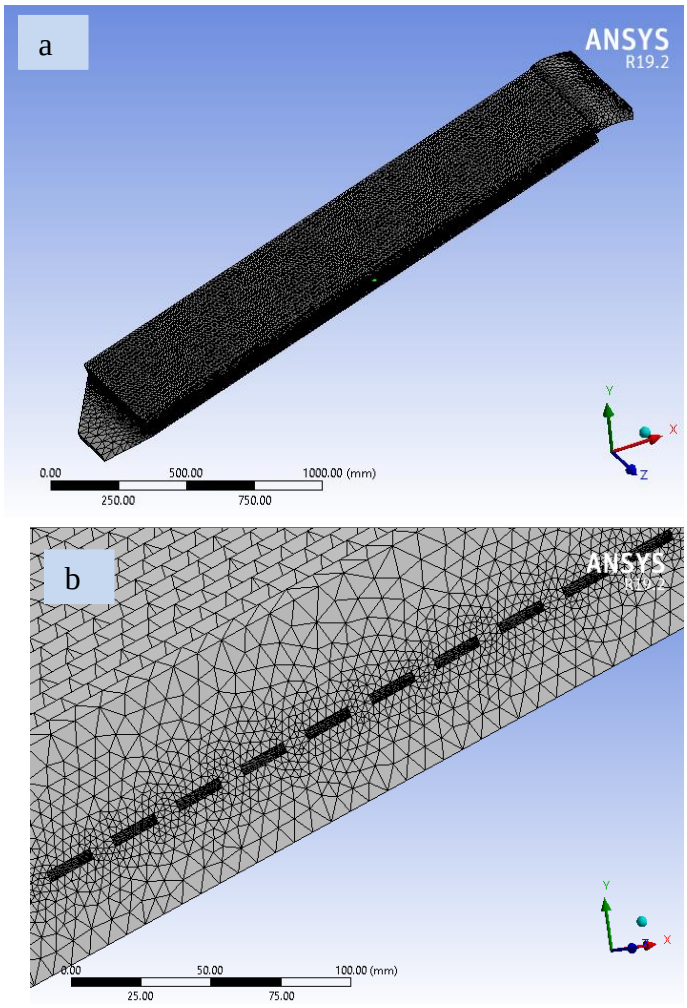

Figure 5. 2 Meshed model for solar collector without (a) and with (b) jet plate.

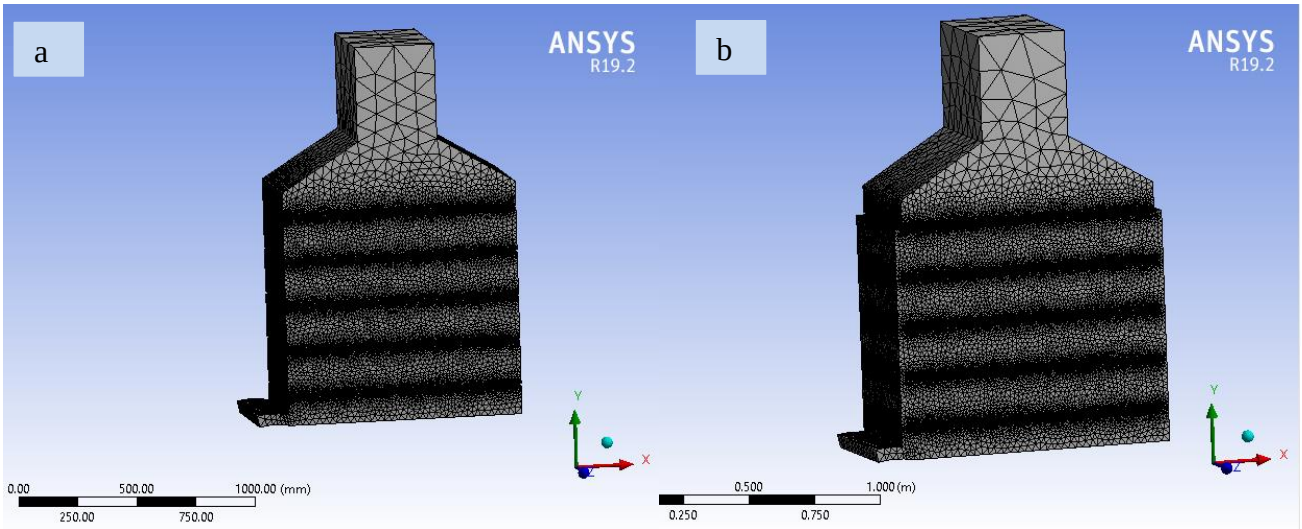

Figure 5. 3 Meshed model for drying chamber without (a) and with header (b).

To obtain better results the entire fluid flow zone is subdivided into many zones and a combination of structured (mapped) and the unstructured mesh was created in the fluid domain. Thus, the grid system has 2,445,779 elements and 475,695 nodes for the collector and 3245776 elements and 654231 nodes for the drying chamber.

5.1.3 Boundary conditions

The boundary condition for different edges has been created while constructing the geometry of the grid in ANSYS ICEM CFD. At the inlet uniform mass flow rates are used and the direction is normal to the opening at the inlet, mass flow rates are taken as $\dot{m}1$= 0.02-0.05 kg/s. The outlet is given as pressure outlet boundary condition with pressure being equal to atmospheric pressure is applied at the exit. Uniform heat flux 500-800 W/m^2 imposed on the absorber which is equal to solar insolation, while all other walls are set to adiabatic. The absorber plate material is taken as aluminum and inside air temperature of the duct is 300K is taken. No-slip boundary condition is given along the wall. The working fluid is dry air and properties are set to be constant and taken based on the inlet temperature and pressure. Turbulence parameters at the inlet are defined using turbulence intensity (5%). Ambient temperature for radiation from the top of the glass is taken as 300 K.

5.1.4 Governing Equations

Computational fluid dynamics governing equations are used to investigate the interactive motion of a large number of individual particles inside the fluid domain. Which defines various parameters e.g. velocity, pressure, Temperature at an individual point inside the fluid domain. Governing equations are non –linear partial differential equations, which governs the flow of fluid and derived from basic physical laws. The principle governing equations used are as follows:

Continuity equation

$$\frac{\partial u}{\partial x}+\frac{\partial v}{\partial y}+\frac{\partial w}{\partial z}=0 \tag{5.1}$$

X- Momentum equation

$$u\frac{\partial u}{\partial x}+v\frac{\partial v}{\partial y}+w\frac{\partial w}{\partial z}=-\frac{1}{\rho}\frac{\partial p}{\partial x}+u\left[\frac{\partial^2 u}{\partial x^2}+v\frac{\partial^2 u}{\partial y^2}+w\frac{\partial^2 u}{\partial z^2}\right] \tag{5.2}$$

Y- Momentum equation

$$u\frac{\partial u}{\partial x}+v\frac{\partial v}{\partial y}+w\frac{\partial w}{\partial z}=-\frac{1}{\rho}\frac{\partial p}{\partial y}+v\left[\frac{\partial^2 v}{\partial x^2}+v\frac{\partial^2 v}{\partial y^2}+w\frac{\partial^2 v}{\partial z^2}\right] \tag{5.3}$$

Z Momentum equation

$$u\frac{\partial u}{\partial x}+v\frac{\partial v}{\partial y}+w\frac{\partial w}{\partial z}=-\frac{1}{\rho}\frac{\partial p}{\partial z}+w\left[\frac{\partial^2 w}{\partial x^2}+v\frac{\partial^2 w}{\partial y^2}+w\frac{\partial^2 w}{\partial z^2}\right] \tag{5.4}$$

Energy equation

$$u\frac{\partial T}{\partial x}+v\frac{\partial T}{\partial y}+w\frac{\partial T}{\partial z}=\alpha\left[\frac{\partial^2 u}{\partial x^2}+v\frac{\partial^2 u}{\partial y^2}+w\frac{\partial^2 u}{\partial z^2}\right] \tag{5.5}$$

In the above equations, u, v and w are the velocity components in x, y and z directions, p and T are the pressure and temperature of the flowing air.

5.2 Solver

The CFD analysis of a solar air heater and dryer is carried out using ANSYS-FLUENT 19.2.

5.2.1 Define material properties:

- ✓ In a solar air heater analysis, the incoming air is assigned a material property as fluid (air) and absorber plate as solid (aluminum).

Table 5.1 Thermo-physical properties of the working fluid & absorber plate

	Material Density (kg/ m^3)	Specific heat J/kg K	Thermal Conductivity (W/m^2K)	Refractive index
Air	1.225	1006	0.0242	--
Glass	2600	840	1.05	1.5
Aluminum	2719	871	202.4	--

5.2.2 Selection of Appropriate Turbulence Model

For selecting an appropriate model for CFD analysis of roughened solar air heater, researchers have carried out validation of various turbulence models. They observed that the results obtained by Renormalization-group (RNG) k-ε model show 72.58% absolute percentage deviation in predicted values and the values calculated from Dittus–Boelter correlations. The results generated from the Realizable k- (model and Standard k- (model are underpredicted, whereas that obtained from Standard k- (model and SST k- (model are overpredicted. Since the results obtained by Renormalization-group (RNG) k- (turbulence model are in good agreement with the Dittus–Boelter and Blasius correlation results, this model was selected for the CFD analysis of a solar air heater since it gives results very close to the experimental results as reported by researchers [45].

Table 5.2 Comparison coefficient of determination (R^2) values of various CFD models [45]

Model	Coefficient of determination(R^2)
Shear Stress Transport (SST) k−ω	0.994
Realizable k−ε	0.995
Standard k−ε	0.996
Renormalization k−ε	0.998

The transport equation for the Realizable *k-ε* model

Turbulent kinetic energy *k* equation [46]

$$\frac{\partial}{\partial t}(\rho\varepsilon)+\frac{\partial}{\partial x_j}(\rho k u_j)=\frac{\partial}{\partial x_j}\left[(\mu+\frac{\mu_t}{\sigma_k})\frac{\partial k}{\partial x_j}\right]+G_k+G_b-\rho\varepsilon-Y_M+S_k \tag{5.6}$$

The rate of energy dissipation *İ* equation,

$$\frac{\partial}{\partial t}(\rho\varepsilon)+\frac{\partial}{\partial x_j}(\rho\varepsilon u_j)=\frac{\partial}{\partial x_j}\left[(\mu+\frac{\mu_t}{\sigma_\varepsilon})\frac{\partial \varepsilon}{\partial x_j}\right]+\rho C_1 S_\varepsilon-\rho C_2\frac{\varepsilon^2}{k+\sqrt{\nu\varepsilon}}+C_{1\varepsilon}\frac{\varepsilon}{k}C_{3\varepsilon}G_b+S_\varepsilon$$

$$Where, C_1=\max\left[0.43,\frac{\eta}{\eta+s}\right],\eta=S\frac{k}{\varepsilon},s=\sqrt{2s_{i,j}{}^2} \tag{5.7}$$

In this equations, G_k represents the generation of turbulence kinetic energy due to the mean velocity gradients, G_b is the turbulence kinetic energy generated due to buoyancy,Y_M represents the contribution of the fluctuating dilatation incompressible turbulence to the overall dissipation rate,C_2 and $C_1\varepsilon$ are the constant, σk and $\sigma\varepsilon$ are the turbulent Prandtl numbers for **k** and ε respectively.S_k and S ε are user-defined source terms. The eddy viscosity is computed from

$$\mu_t=\rho C_\mu\frac{k^2}{\varepsilon}\qquad \text{The model constants are } C_{1\varepsilon}=1.44, C_2=1.9, \sigma_\varepsilon=1.2 \tag{5.8}$$

5.2.3 Prescribe operating parameters

The operating parameters used in the CFD analysis of a solar collector and drying chamber include uniform heat flux (solar irradiance), mass flow rate, jet-to-jet spacing, wind speed, ambient temperature. The geometry of regular inline jet holes arrays can be characterized by X, Y, and Z. X and Y represent the jet-to-jet spacing in stream wise direction and span wise direction respectively in a Cartesian coordinate and Z give the jet-to-absorber plate spacing.

- ✓ For drying chamber, product trays are assumed as a porous media for airflow. Porous media are modeled by the addition of a momentum source term to the standard fluid flow equations. The pressure change was defined as a combination of Darcy's Law and an additional inertial loss term which is given by [47]

$$\Delta p = -\left(\frac{\mu}{\alpha}U_n + C_2\frac{1}{2}\rho U_n^{\,2}\right)\Delta m \qquad (5.8)$$

Where μ is the fluid viscosity, α is the permeability of the tray, C2 is the pressure-jump coefficient (pressure loss coefficient per unit thickness), Un is the velocity normal to the tray, and Δm is the thickness of the tray.

5.3 Solution Procedure

In the present simulation governing equations of continuity, momentum and energy are solved by the finite volume method in the steady-state regime using CFD code ANSYS FLUENT. A second-order upwind scheme is chosen for both energy and momentum equations. The double precision pressure based solver is selected in order to solve a set of equations used. Second order upwind discretization scheme is selected for all the transport equations. The governing equations for mass and momentum conservation are solved with a segregated approach in steady state, where equations are sequentially solved with implicit linearization. The SIMPLE algorithm (semi-implicit method for pressure linked equations) is chosen as a scheme to couple pressure and velocity.

Initialization

Before we start our calculations or patch initial values for selected variables in selected cells we must initialize the flow field in the entire domain. The Solution Initialization Task Page allows us to set initial values for the flow variables and initialize the solution using these values. Initialization will result in the volume fraction, X, Y, and Z velocities, and pressure being patched in the domain. The volume fraction will be patched in the domain based on the the free surface level of the selected zone from the Compute from the list. The velocities in the domain will be patched assuming the constant value provided for the velocity magnitude in the selected zone[4].

The general assumption, consider in the analysis are as follows:

1. The flow is steady, two dimensional, turbulent and fully developed.

2. The flow is single phase across the duct.

3. The walls in contact with the fluid are assigned no-slip boundary condition.

4. The duct wall, absorber plate, and roughness material are homogeneous and isotropic. The thermodynamic properties of air and the absorber plate (aluminum) are considered constant.

5. The effect of radiation heat transfer and other heat losses are considered

The convergence criteria of 10^{-6} for the residuals of the continuity equation, 10^{-6} for the residuals of the momentum the equation, 10^{-3} for the residuals of the velocity components and10^{-6} for the residuals of the the energy equation is assumed. The heat transfer coefficient at the solid-fluid interface was also monitored to assure the convergence of the solution.

CHAPTER SIX

5 RESULTS AND DISCUSSION

5.1 Solar collector

Three-dimensional steady-state CFD simulation of heat transfer and fluid flow characteristics has been carried out at different mass flow rate conditions and at constant heat flux input at 600 W/m^2 for v-corrugated solar collector without and with jet impingement for jet diameter of 6,8,10 mm and drying chamber with and without header in ANSYS FLUENT 19.2. The results of simulation are presented and compared with conventional V-corrugated absorber plate. The enhancement of thermal performance for variable mass flow rate is discussed follows. Results show the velocity distribution, temperature distribution in the plane taken parallel to direction of air flow for all conditions generated using CFD post processors.

The thermal performance of a solar air heater was investigated in terms of outlet temperature and efficiency with the different working condition also with different mass flow rate. The velocity vector represents the flow distribution and the temperature contour shows the temperature distribution inside solar collector for different configurations.

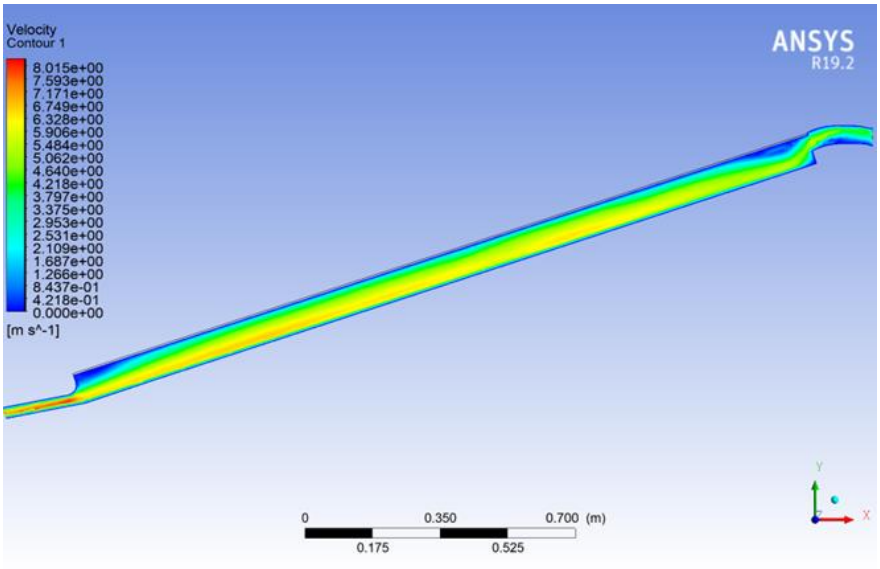

Figure 6. 1 The contour plot of velocity without jet for the mass flow rate of 0.05kg/s

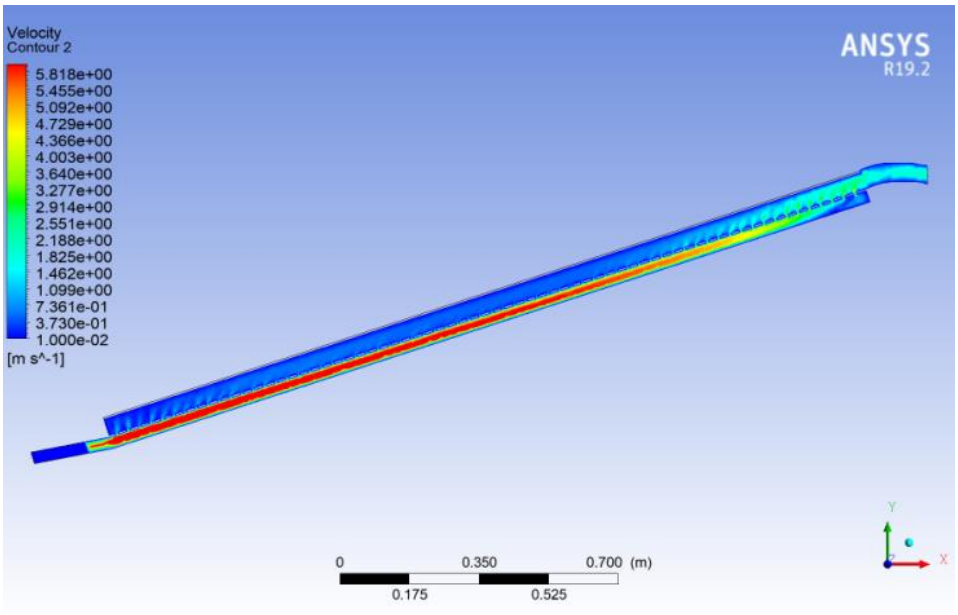

Figure 6. 2 The contour plot of velocity D=8 mm for the mass flow rate of 0.05kg/s

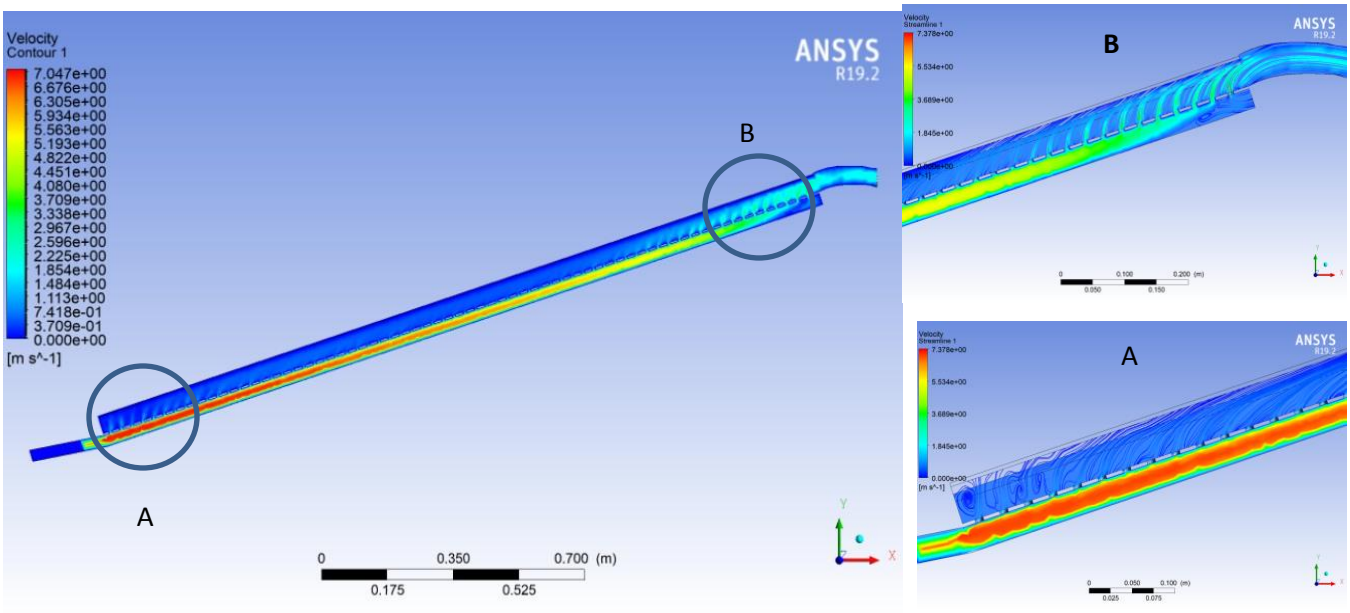

Figure 6. 3 The contour plot of velocity D=6 mm for the mass flow rate of 0.05kg/s

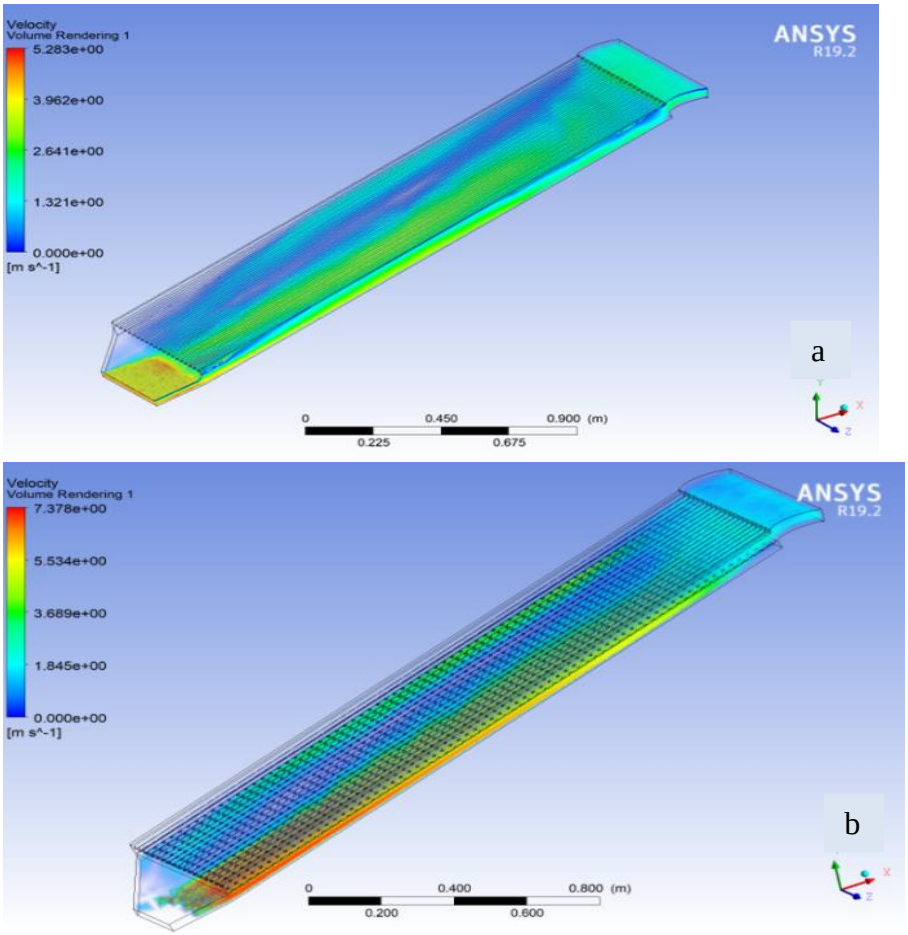

Figure 6. 4 The 3-D contour plot of velocity without jet and D=6 mm for a mass flow rate of 0.05kg/s

Error! Reference source not found. to **Error! Reference source not found.** shows the 2D and 3D velocity contour of solar collector for without jet plat, D=8 mm, D=6 mm. The velocity of air near the jet plate is very high and it decreases with increasing distance from the inlet wall. Velocity contour as shown in **Error! Reference source not found.** high-velocity jet of air impinging onto the bottom surface of the absorbing plate. This impinging action results in an increased cooling effect on the absorber plate and leads to improved heat transfer to the flowing air. For D=6 mm, the jet plate creates high-velocity air jet that impinges on the absorber plate and continues to flow at a relatively higher velocity below the absorber plate which results in higher heat transfer coefficient and hence higher Nusselt number.

From Error! Reference source not found. it is seen that for the collector with the jet plate the flow distribution is not properly uniform throughout the absorber plate as a result of pressure fluctuation and viscous effect. A jet flow is shown near to the absorber through jet plat. This jet type flow is able to increase the heat transfer phenomenon with the increasing forced convection heat transfer coefficient.Air velocity passing across the collector is increased with jet plate compare to without jet plate. Due to turbulence created in jet plate region air velocity increases and which enhances the heat transfer coefficient.

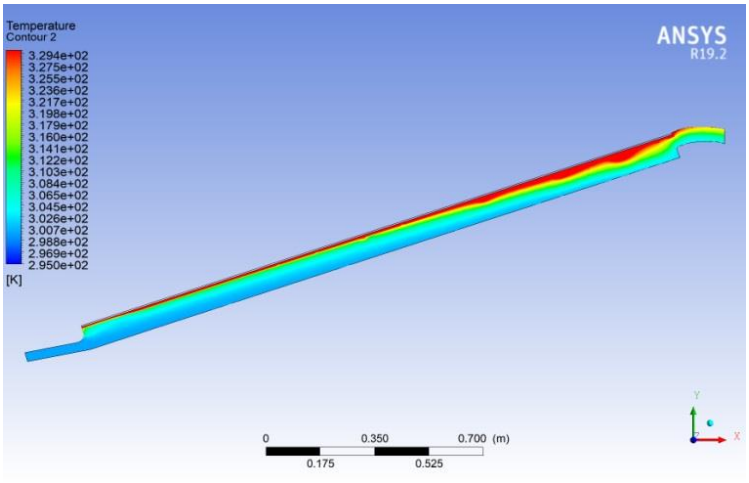

Figure 6. 5 Temperature contour of collector without jet plate

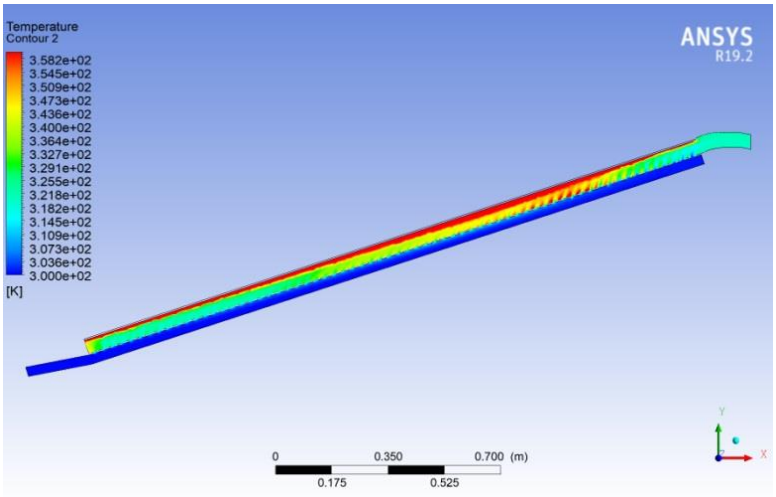

Figure 6. 6 Temperature contour of collector D=10 mm jet plate.

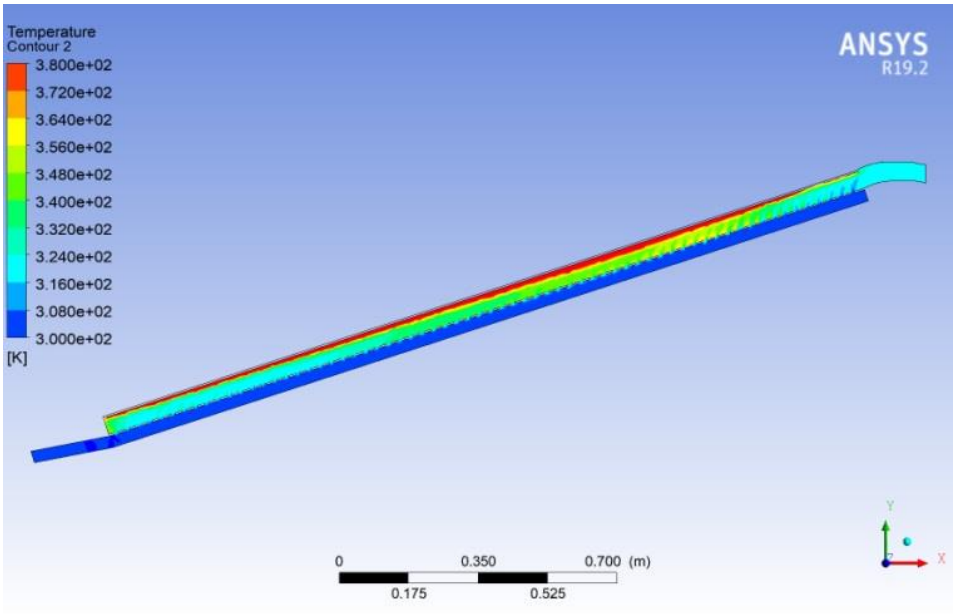

Figure 6. 7 Temperature contour of collector D=8 mm jet plate.

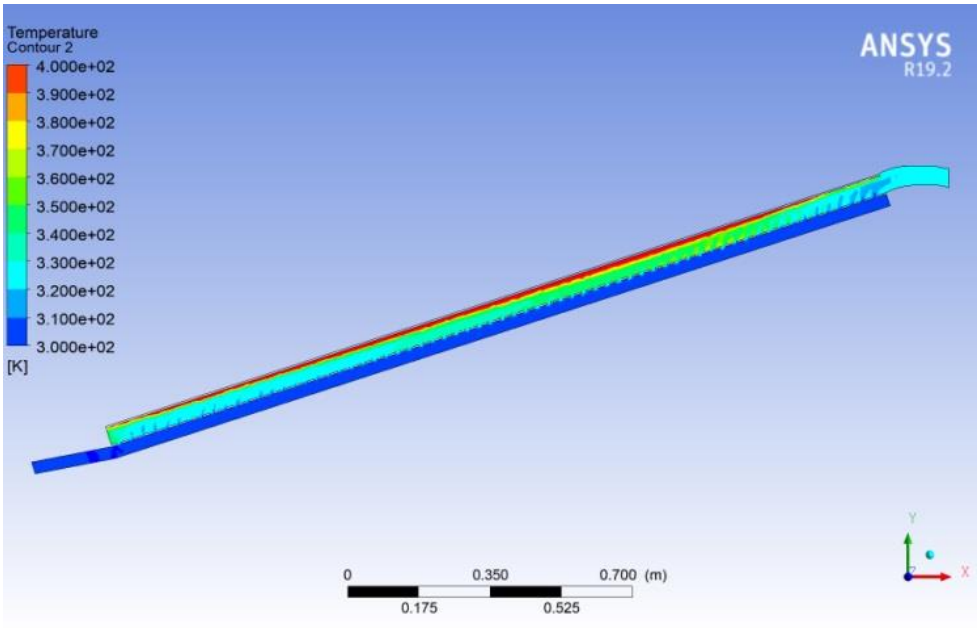

Figure 6. 8 Temperature contour of collector D=6 mm jet plate.

From Error! Reference source not found. to Error! Reference source not found. the temperature contour inside solar collector is displayed. The air coming out from the jet strikes the absorber plate, and it prompts the higher heat removal from the absorber plate as opposed to the air simply streaming over the absorber plate. Likewise, it makes the turbulent stream and results in the

higher outlet air temperature. The absorber plate had a normal temperature of 300°C at the entering point of the air. Hence, the temperature gradually increased to 329,358, 380, and 400 K for the mass flow rate of 0.05 kg/s for without jet plate, 10,8,6 mm diameter of jet plate respectively. The air above the jet plate takes the largest amount of heat at the point of entering then the air decreases its heat absorption capacity so that the temperature is raised from the entering to the exit point. There is a high heat removal rate for 6 mm diameter of the jet plate due to high turbulence created through nozzle flow.

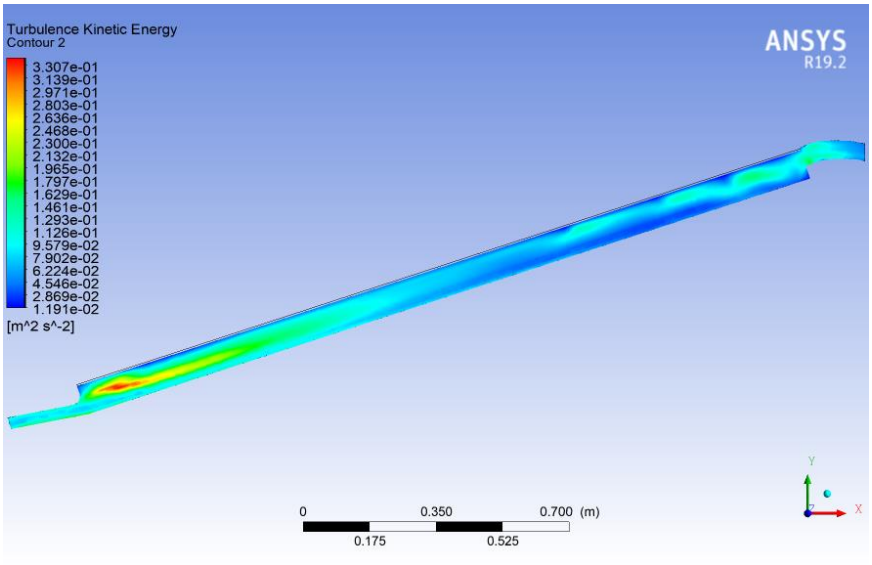

Figure 6.8 1 Contour of turbulent kinetic energy for collector without a jet plate

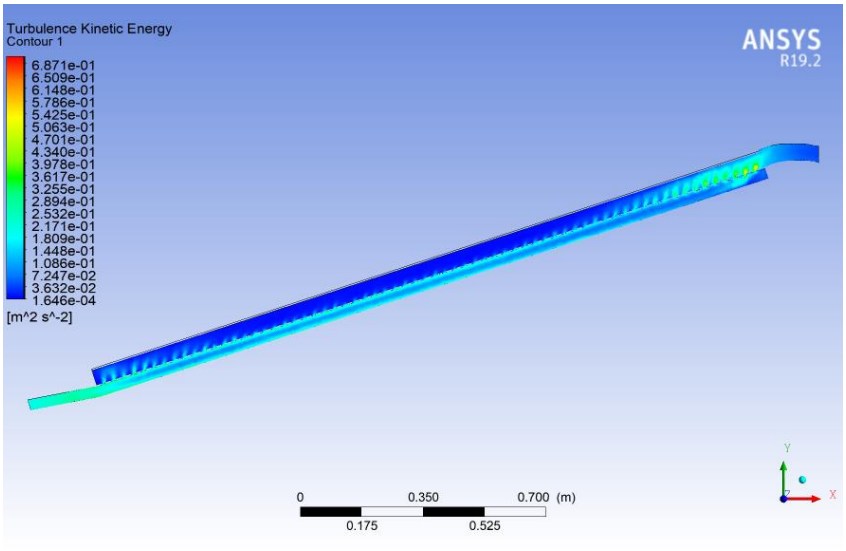

Figure 6. 9 Contour of turbulent kinetic energy for collector D=6 mm jet plate.

Figure 6.8 1 and **Error! Reference source not found.** shows the contour of turbulent kinetic energy for collector without a jet plate and D=6 mm jet plate. It can be seen that the peak value of the turbulent intensity is found 0.687 m^2/s^2 near the exit of the collector on the top side of the jet plate for the collector with jet impingement on corrugated absorber plate and 0.33 m^2/s^2 the collector without a jet plate. The intensity of turbulent kinetic energy decreases as the distance from the wall increases reveals that the turbulent intensity is relatively higher in the outlet region as well as in the regions close to the jet plate where flow impingement takes place. Thus, it is found that the combined effect of formation of high velocity along with flow impingement effect and flow acceleration near the absorber surface leads to increased heat transfer rate. As a result, the instances of flow impingement, and flow acceleration zones are also higher which leads to enhanced heat transfer to the flowing air stream.

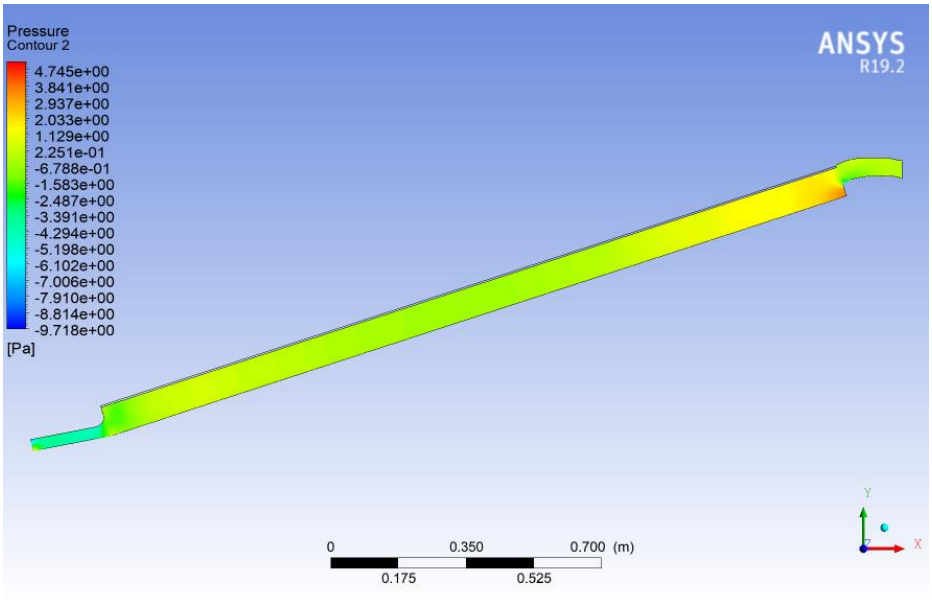

Figure 6. 10 Contour of pressure for collector without a jet plate.

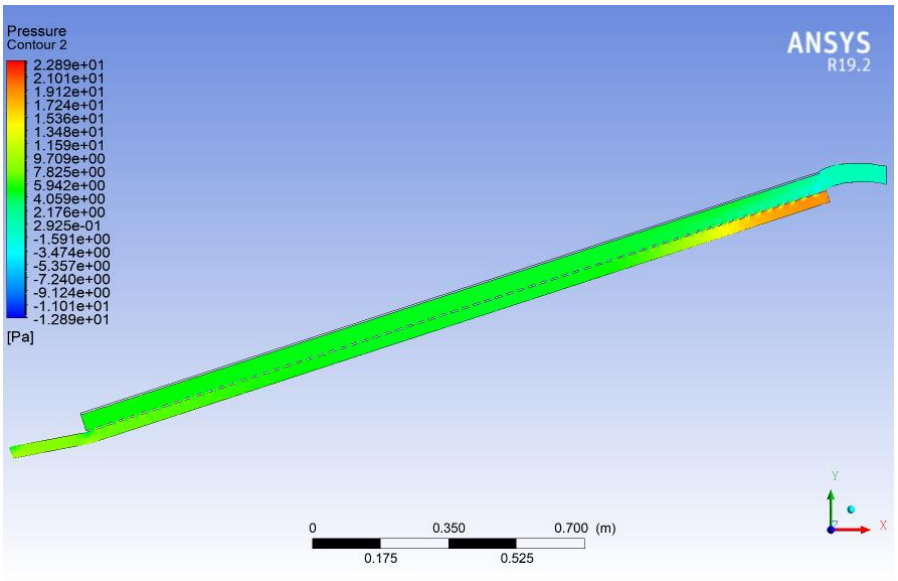

Figure 6. 11 Contour of pressure for collector D=6 mm jet plate.

Error! Reference source not found. and Error! Reference source not found. shows the contour of pressure for collector without a jet plate and with D=6 mm jet plate. The pressure distribution across the length of the collector is 4.7 and 22.8 Pa for solar collector without a jet plate and with D=6 mm jet plate respectively. So the pressure drop for the collector with the jet plate is higher. This is due to high turbulence created as a result of the jet plate and high-pressure drop is created at the bottom of the jet plate.

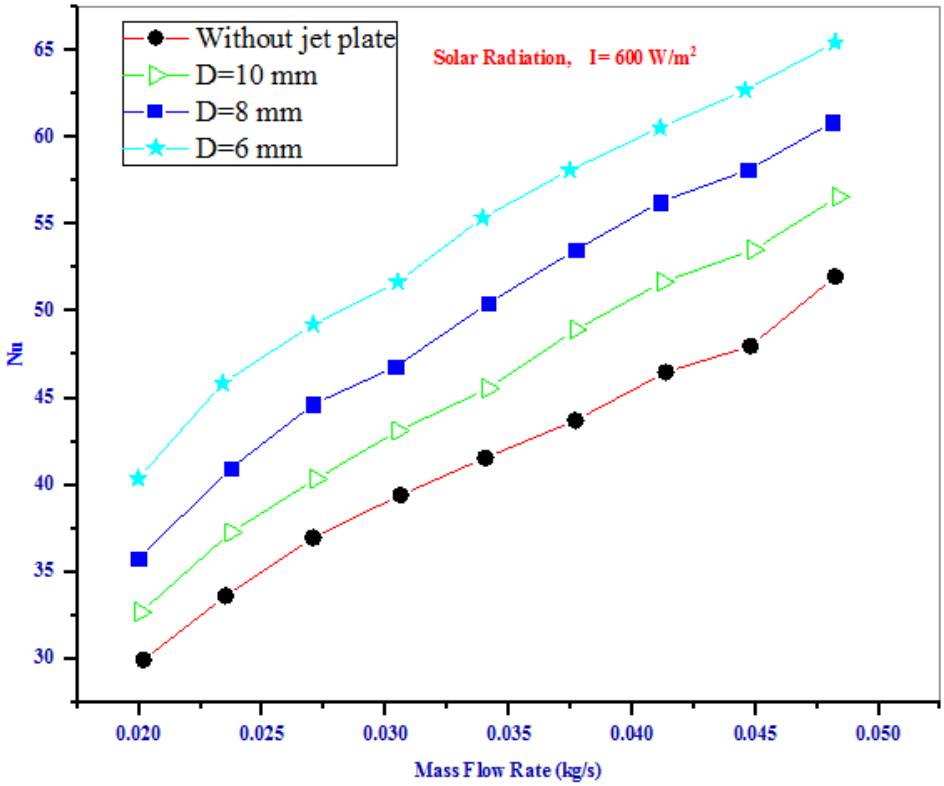

Figure 6. 12 Variation of Nusselt number with a mass flow rate

Error! Reference source not found. shows the Variation of Nusselt number with mass flow rate for 6,8,10 mm jet diameter and without jet plate V-corrugated absorber plate, Nusselt number increases with increasing mass flow rate. This is due to the fact that as the mass flow rate increases the rate of heat transfer from the absorber plate increases resulting in higher values of Nusselt number. But it is observed that the value of Nusselt number is more in D=6 mm jet diameter on corrugated absorber plate as compared to others. This is further validated by the variation of the temperature at different air flow rate conditions as shown in **Error! Reference source not found.**. It is clear that the temperature decreases with an increase in the mass flow rate of air to increase heat transfer coefficients

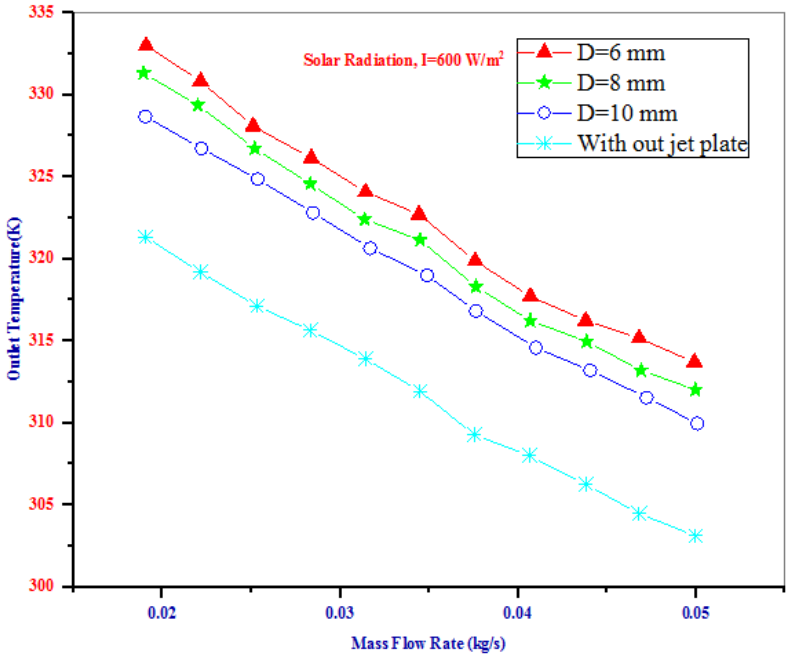

Figure 6. 13 *Variation of Outlet temperature with a mass flow rate*

Error! Reference source not found. shows the Variation of Outlet temperature with mass flow rate for 6,8,10 mm jet diameter and without jet plate V-corrugated absorber plate, Temperature decreases with increasing mass flow rate. It is noticed that at higher flow rate the output temperature is almost similar for all the collectors. But for the lower flow rate, the D=6 mm collector clearly provides a better output with the maximum temperature of 333 K. Another observation in **Error! Reference source not found.** is that all jet pate collectors have a better thermal performance with a mass flow rate. This indicates better productivity through the jet plate with v-groove corrugated absorber plate compared to solar collector without a jet plate.

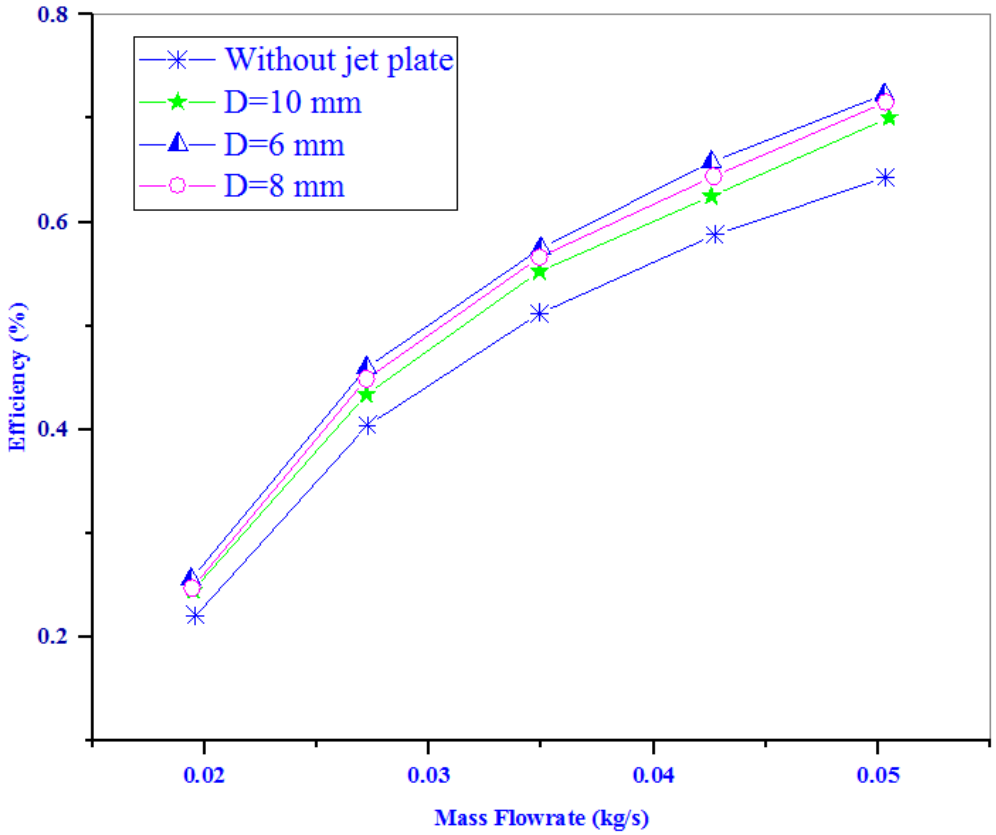

Figure 6. 14 Variation of efficiency with mass flow rate at a different jet diameter

It is observed from **Error! Reference source not found.** that represents the variation of thermal efficiency with reference to mass flow rate for the four types of collectors. It is quite evident from the curve the efficiency is increased with an increase in mass flow rate values for all jet diameters and without the jet. The V-corrugated collector without jet plate has a maximum efficiency of 64.3 %, and the maximum efficiency of 72.3% can be seen at a jet diameter of 6 mm. It is concluded from the results that v-groove 6 mm diameter of jet plate collector has the highest efficiency value due to the larger contacting area created by the v-groove absorber and high turbulence created by the jet plate.

6.2 Validation of CFD Results

To validate the present numerical model, the results are compared with experimental results of different geometries of similar trends for efficiency with Alsanossi M. Aboghrara et.al [37] as shown in **Error! Reference source not found.**. It can be seen that there show good agreement with experimental and CFD work. It has been observed that the proposed model of jet impingement on corrugated absorber plate predicts the experimental data quite accurately.

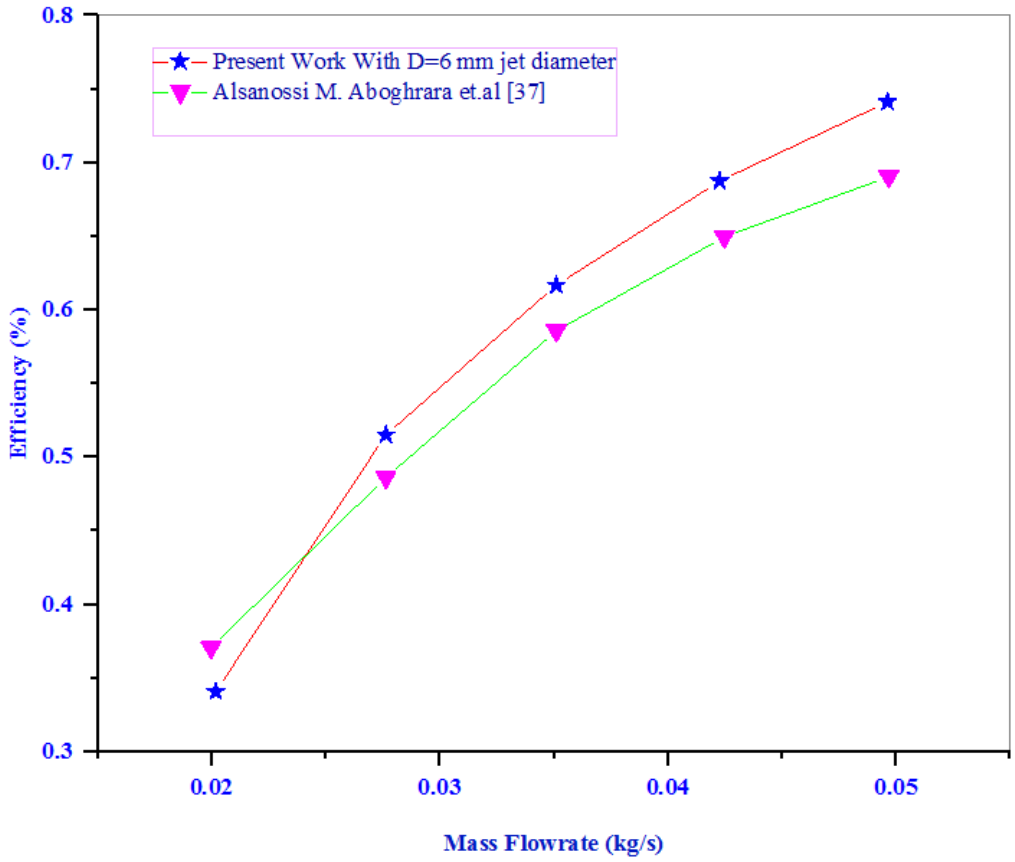

Figure 6. 15 Validation of CFD Results

6.3 Drying chamber

The drying chamber is modeled without header and with front and back header with dimension 1 m × 1 m × 1.5 m (width, length, and height, respectively). The dryer system consists of 5 trays system. The end space in the drying chamber is used to occupy the operator for loading or unloading the product to the last column of trays. In this process, the aim is to visualize the air velocity and temperature distribution inside the whole dryer, specifically throughout trays to predict the drying uniformity. The pattern of the air stream in the drying chamber is important and since there was no variable condition in this study, the simulation was carried out in steady state condition. Only half of the drying chamber was analyzed since the shape is symmetry by defining the symmetry surface to the middle boundary. The symmetry plane was selected to study and analyze the velocity and temperature in the drying chamber.

The set-up of boundary conditions was defined as followings:

- ✓ Inlet: air velocity of 2.5 /s and an air temperature of 333 K which is outlet temperature of a solar collector with 6 mm jet diameter.
- ✓ Outlet: Assuming gauge pressure=0 at the outlet.
- ✓ Trays: The trays were assumed as porous media with 10% porosity.
- ✓ Wall: Heat transfer coefficient of the chamber wall and environmental conditions were defined. The environment temperature is assumed at 300 K. The bottom surface is assumed as no heat loss.

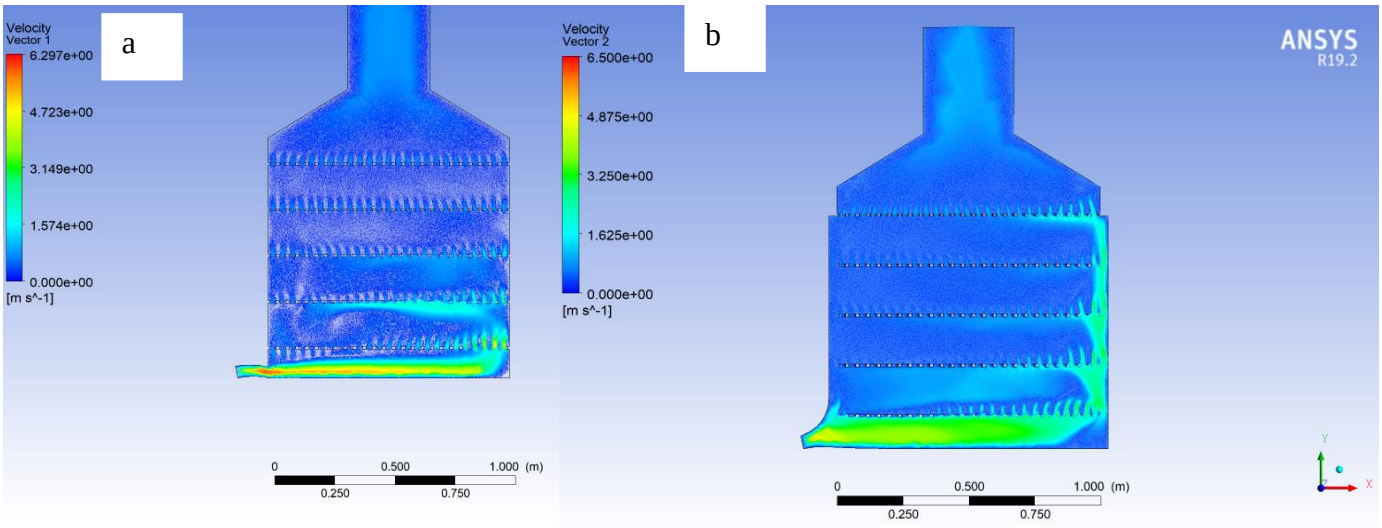

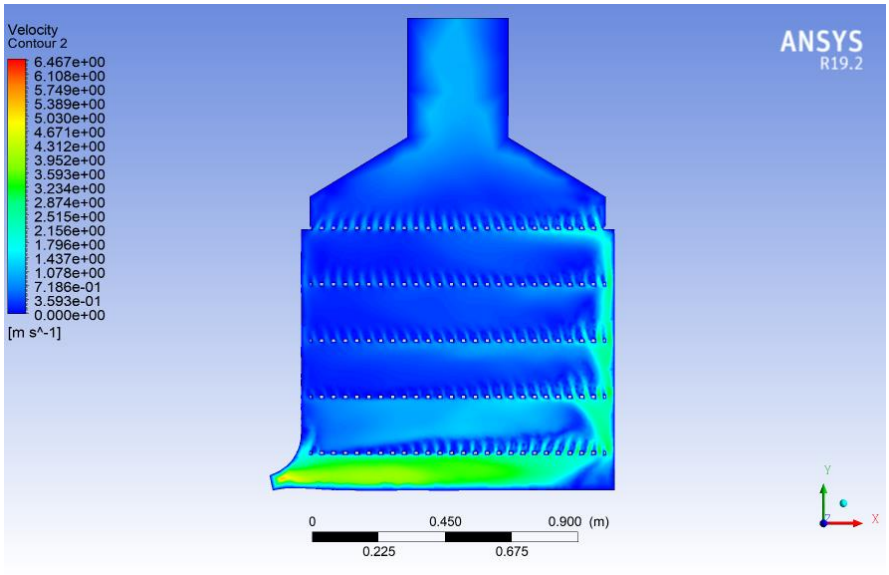

Figure 6. 16 Velocity distribution profiles for without (a) and with (b) header at symmetry plane

It might be noticed from **Error! Reference source not found.** that the velocity of the air is high at the inlets compared to the rest locations. For example, the velocity of the air entering from the inlet 1 is between 2 and 5 m/s where it decreases progressively as long as it moves

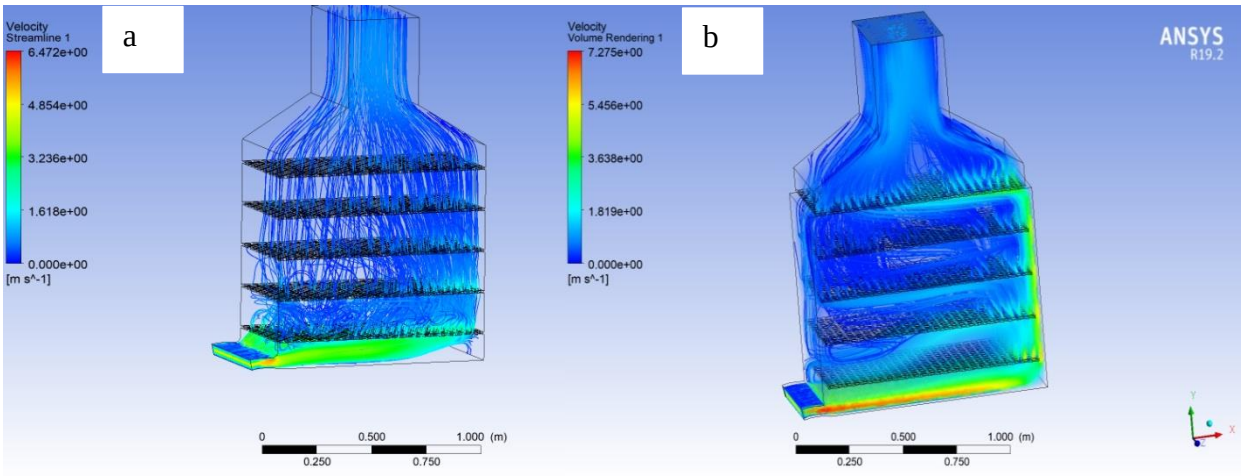

trays inside the chamber.

Figure 6. 17 3D streamline for without (a) and with (b) header in the drying chamber.

The high intensity of the air in the drying chamber is a desirable feature in order to remove more moisture from products. From the Error! Reference source not found.**,** it is easy to see that the velocity of air streamlines ranges from 0 to 3.2 m/s for drying chamber without header and 0 to 5.4 m/s except for the inlet and exit domain**.**

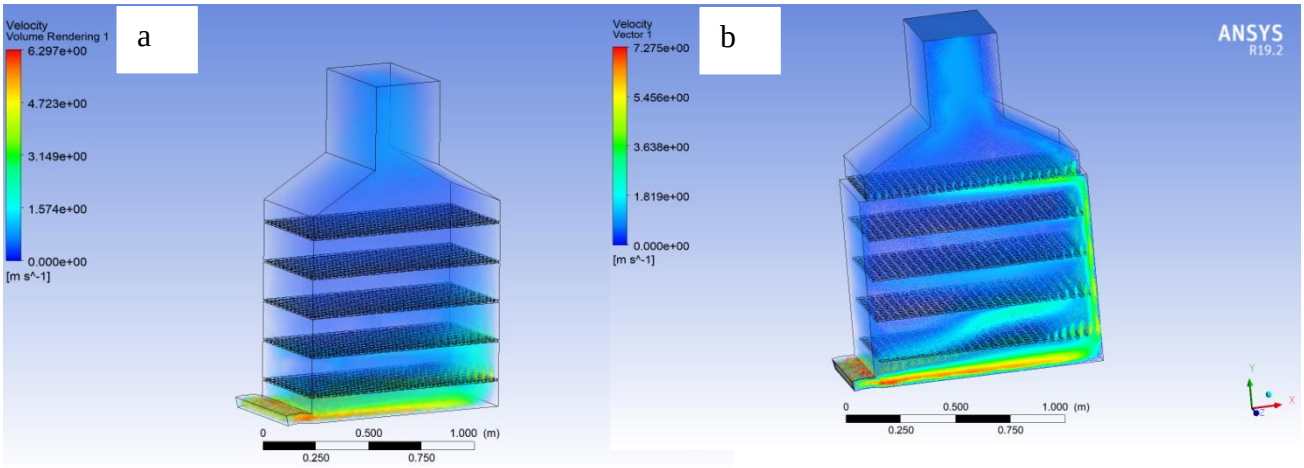

Figure 6. 18 3D volume rendering for without (a) and with (b) header of drying chamber

The air velocity above the trays are very important to carries the moisture from the product. The air velocity along the trays at the symmetry plane was studied in this simulation. The air velocity profile inside the drying chamber without and with the header is shown from **Error! Reference source not found.** to Generally, the average air velocities for drying chamber with the header is somewhat uniform and more velocity around the trays which is 1.8 to 3.6 m/s and the bottom tray has higher velocity for both cases since the positions are close to the inlet. For drying chamber a ıt header as the drying air passes over the trays, the air velocity would de b create non-uniform drying rate. The minimum air velocity above the tray is around 1.1 m/s at the left side of the tray. The high velocity at the first trays can't be avoided because it closes to the inlet with a maximum velocity of 3.9 m/s. The variation of the final moisture content of the product may occur based on the velocity profile. The high air velocity at the above product (tray) will make the product dry faster compared to the product with low air velocity.

The simulation result of 3D streamline is shown in **Error! Reference source not found.** on the streamline color; it shows that the air velocity is higher at the areas that close to the inlet for both cases. The air velocity is low along the tray for drying chamber without header because the air was distributed to all the trays at different levels. The average air velocity at the bottom tray is highest because it closes to the air inlet.

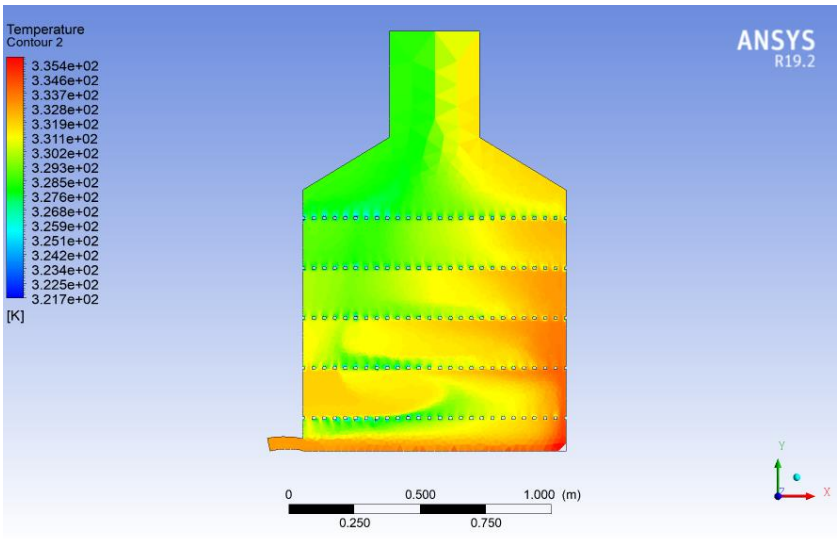

Figure 6. 19Temperature distribution profiles at the symmetry plane for drying chamber without header.

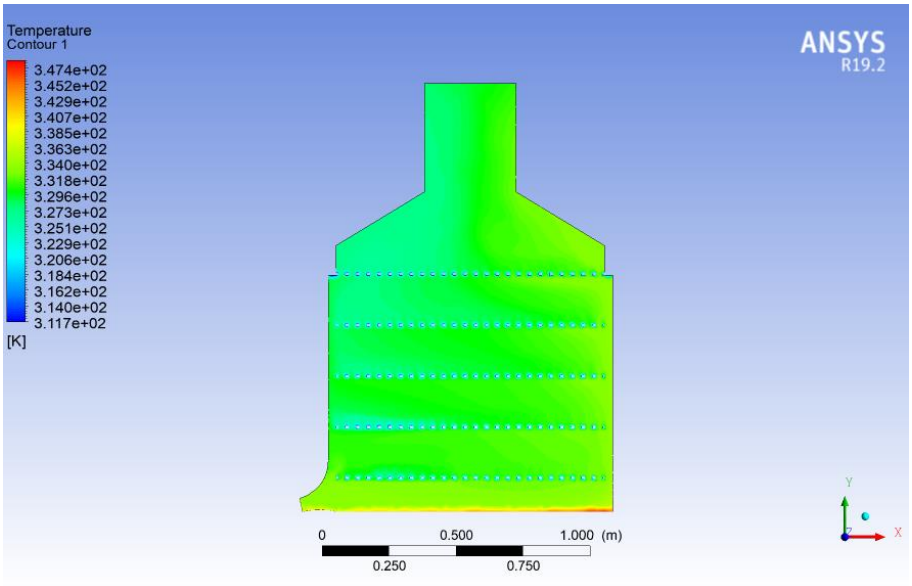

Figure 6. 20 Temperature distribution profiles at the symmetry plane for drying chamber with header

As can be seen from Error! Reference source not found. and Error! Reference source not found. Temperature distribution profiles at the symmetry plane for the drying chamber without and with the header is displayed. The maximum temperature given is around 333 K which is at the inlet of the drying chamber whereas the lowest temperature is 321 K. It could be observed that the temperature inside the chamber along the trays. It was found that the temperature for most of the trays was in the range of 321 to 333 expect half of the upper tray for both drying chambers. The temperature for the upper tray was in the range of 328.5 K to 330.2. for both drying chamber it might be seen that the bottom trays towards the inlet achieve the highest temperature and for drying chamber with a header as it can be seen the temperature profiles in the drying chamber can be considered as uniform because the air is uniformly distributed from front and back header.

The change in the behavior of the air flow in the dryer has a direct impact on the efficiency; these changes increase the moisture transfer of the grain to the environment, which is reflected in a significant reduction in the drying time. The reduction of the drying time is an aspect of great interest in terms of productivity, this reduction of time is translated in the decrease in costs of drying. It´s necessary to point out the temperature distribution obtained was satisfactory due to the high uniformity inside the chamber by placing the front and back header in the drying chamber.

CHAPTER SEVEN

CONCLUSIONS AND RECOMMENDATIONS

7.1 CONCLUSIONS

The 3-D CFD analysis of solar air heater with and without jet impingement on corrugated absorber plate and drying chamber has been carried out. The effect of jet diameter and mass flow rate on heat transfer enhancement and air distribution in the drying chamber is studied. On the basis of the above investigation and results obtained following are the major conclusions:

- CFD has been applied in the design of a solar air heater. The quality of the solutions obtained from CFD simulations is largely within the acceptable range providing that CFD is an effective tool for predicting the behavior and performance of a solar air heater.
- Jet impingement on corrugated absorber plate is an effective technique to enhance the rate of heat transfer as compared to corrugated absorber plate solar air heaters. It has been found that thermal efficiency increases with the increase in breakage of the laminar sub-layer create higher turbulence of air, which results in higher heat transfer. It was found that by using modified air heater thermal efficiency increased by 8.0 %.
- Nusselt number enhancement of jet impingements on corrugated absorber plate with an increase in mass flow rate due to an increase in heat transfer surface area and turbulence. It gives nusselt number of 27-45 for without jet plate and 40-60 for the jet plate.
- The efficiency increases with increasing air mass flow rate. This is because the heat transfer capacity depends directly on the mass flow rate, which induces higher velocities through the jet plate and more heat transfer from the absorber plate to the air.
- The maximum thermal efficiency 72.3 % is achieved on corrugated absorber plate with a jet diameter of 6 mm and a mass flow rate of 0.05 kg/s.
- It´s necessary to point out the temperature distribution obtained was satisfactory due to the high uniformity inside the chamber by placing the front and back header in the drying chamber. Good airflow distribution throughout the drying chamber can improve the drying uniformity.

7.2 RECOMMENDATIONS

Based on the literature review and discussed in this work, following suggestions and recommendations have been made to extend the research work on jet impingement on corrugated absorber plate for drying application.

- As the drying air is exhausted to the surrounding so, one can study the recirculation of the drying air to improve the thermal efficiency of the drying chamber.
- A computer simulation models to simulate the short and long terms performance of the drying systems with and without the storage material to estimate the solar drying curves of the dried products and study the cost benefits of the solar drying of agricultural products.
- It is recommended that the jet impingement on a corrugated absorber plate can be used for space heating and solar drying. So, these benefits must be studied experimentally.

REFERENCE

[1] W. Gao, W. Lin, T. Liu, and C. Xia, "Analytical and experimental studies on the thermal performance of cross-corrugated and flat-plate solar air heaters," *Appl. Energy*, vol. 84, no. 4, pp. 425–441, 2007.

[2] O. Prakash, V. Laguri, A. Pandey, A. Kumar, and A. Kumar, "Review on various modelling techniques for the solar dryers," *Renew. Sustain. Energy Rev.*, vol. 62, pp. 396–417, 2016.

[3] P. Ghosh and N. Venkatachalapathy, "Processing and Drying of Coffee – A Review," *Int. J. Eng. Res. Technol.*, vol. 3, no. 12, pp. 784–794, 2014.

[4] A. P. Singh and O. P. Singh, "Performance enhancement of a curved solar air heater using CFD," *Sol. Energy*, vol. 174, no. February, pp. 556–569, 2018.

[5] A. Saxena, Varun, and A. A. El-Sebaii, "A thermodynamic review of solar air heaters," *Renew. Sustain. Energy Rev.*, vol. 43, pp. 863–890, 2015.

[6] P. Singh Chauhan, A. Kumar, and P. Tekasakul, "Applications of software in solar drying systems: A review," *Renew. Sustain. Energy Rev.*, vol. 51, pp. 1326–1337, 2015.

[7] M. Mohanraj and P. Chandrasekar, "Performance of a solar drier with and without heat storage material for copra drying," *Int. J. Glob. Energy Issues*, 2009.

[8] S. R. Toshniwal, U. and Karale, "A review paper on Solar Dryer," *Int. J. Eng. Res. Appl.*, 2013.

[9] T. Rajaseenivasan, S. Ravi Prasanth, M. Salamon Antony, and K. Srithar, "Experimental investigation on the performance of an impinging jet solar air heater," *Alexandria Eng. J.*, vol. 56, no. 1, pp. 63–69, 2017.

[10] A. Singh Yadav and J. Bhagoria, "International Journal of Ambient Energy Numerical investigation of flow through an artificially roughened solar air heater Numerical investigation of flow through an artificially roughened solar air heater," *Int. J. Ambient Energy*, vol. 36, no. 2, pp. 87–100, 2015.

[11] E. J. Amir, K. Grandegger, A. Esper, M. Sumarsono, C. Djaya, and W. Mühlbauer,

"Development of a multi-purpose solar tunnel dryer for use in humid tropics," *Renew. Energy*, vol. 1, no. 2, pp. 167–176, 1991.

[12] H. C. Chen *et al.*, "Effect of roughness element pitch on heat transfer and friction characteristics of artifical roughened solar air heater duct," *Renew. Energy*, vol. 2, no. 2, pp. 175–183, 2012.

[13] R. K. Nayak and S. N. Singh, "Effect of geometrical aspects on the performance of jet plate solar air heater," *Sol. Energy*, 2016.

[14] T. Alam and M. H. Kim, "Performance improvement of double-pass solar air heater – A state of art of review," *Renewable and Sustainable Energy Reviews*, vol. 79. pp. 779–793, 2017.

[15] A. P. Omojaro and L. B. Y. Aldabbagh, "Experimental performance of single and double pass solar air heater with fins and steel wire mesh as absorber," *Appl. Energy*, vol. 87, no. 12, pp. 3759–3765, 2010.

[16] M. A. Karim and M. N. A. Hawlader, "Performance investigation of flat plate, v-corrugated and finned air collectors," *Energy*, 2006.

[17] M. N. Metwally, H. Z. Abou-Ziyan, and A. M. El-Leathy, "Performance of advanced corrugated-duct solar air collector compared with five conventional designs," *Renew. Energy*, vol. 10, no. 4, pp. 519–537, 1997.

[18] Y. Shi, M. B. Ray, and A. S. Mujumdar, "Computational study of impingement heat transfer under a turbulent slot jet," *Ind. Eng. Chem. Res.*, vol. 41, no. 18, pp. 4643–4651, 2002.

[19] K. E. J. Al-Juamily, A. J. N. Khalifa, and T. A. Yassen, "Testing of the performance of a fruit and vegetable solar drying system in Iraq," *Desalination*, 2007.

[20] V. M. Romero, E. Cerezo, M. I. Garcia, and M. H. Sanchez, "Simulation and validation of vanilla drying process in an indirect solar dryer prototype using CFD Fluent program," in *Energy Procedia*, 2014.

[21] P. Krawczyk *et al.*, "33) SUN AND SOLAR DRYING , TECHNIQUES AND

EQUIPMENT II . SOLAR DRYING II . 1 . Types of Solar Dryers," *Renew. Sustain. Energy Rev.*, 2012.

[22] G. Çakmak and C. Yildiz, "Design of a new solar dryer system with swirling flow for drying seeded grape," *Int. Commun. Heat Mass Transf.*, 2009.

[23] R. Karwa and G. Chitoshiya, "Performance study of solar air heater having v-down discrete ribs onabsorber plate," *Energy*, 2013.

[24] A. Boulemtafes-Boukadoum and A. Benzaoui, "CFD based analysis of heat transfer enhancement in solar air heater provided with transverse rectangular ribs," *Energy Procedia*, vol. 50, pp. 761–772, 2014.

[25] K. Kumar, D. R. Prajapati, and S. Samir, "Heat transfer and friction factor correlations development for solar air heater duct artificially roughened with 'S' shape ribs," *Exp. Therm. Fluid Sci.*, 2017.

[26] H. T. Ebuy, "SIMULATION OF SOLAR CEREAL DRYER USING TRNSYS School of Graduate Studies Mechanical Engineering Program SIMULATION OF SOLAR CEREAL DRYER USING," 2007.

[27] "Horizon Plantations PLC." [Online]. Available: https://horizonplantations.com/limmu-horizon.html. [Accessed: 13-Nov-2018].

[28] "Solar Irradiance - calculate the solar energy available on your site." [Online]. Available: http://solarelectricityhandbook.com/solar-irradiance.html. [Accessed: 22-Nov-2018].

[29] C. F. F. Karney, R. E. Deakin, and R. E. Deakin, "F.W. Bessel (1825): The calculation of longitude and latitude from geodesic measurements," *Astron. Nachrichten*, vol. 331, no. 8, pp. 852–861, Sep. 2010.

[30] S. A. M. Maleki, H. Hizam, and C. Gomes, "Estimation of hourly, daily and monthly global solar radiation on inclined surfaces: Models re-visited," *Energies*, vol. 10, no. 1, 2017.

[31] "Solar Panel Orientation and Positioning of Solar Panel." [Online]. Available: http://www.alternative-energy-tutorials.com/solar-power/solar-panel-orientation.html.

[Accessed: 22-Nov-2018].

[32] I. O. Onigbogi, S. S. Sobowale, and O. S. Ezekoma, "Design, Construction and Evaluation of a Small Scale Solar Dryer," *J. Eng. Appl. Sci.*, 2012.

[33] S. L. Lanhua DAI, "Simulation of hourly solar radiation on tilted surface at Dalian in China," *Int. Conf. Clean Energy*, no. April, 2012.

[34] B. Y. H. Liu and R. C. Jordan, "A Rational Procedure for Predicting The Long-Term Average Performance of Flat-Plate Solar-Energy Collectors With Design Data for the U. S., Its Outlying Possessions and Canada*," *Sol. Energy*, 1963.

[35] C. A. Gueymard, "A review of validation methodologies and statistical performance indicators for modeled solar radiation data: Towards a better bankability of solar projects," *Renew. Sustain. Energy Rev.*, 2014.

[36] T. Hong, C. Koo, and T. Kwak, "Framework for the implementation of a new renewable energy system in an educational facility," *Appl. Energy*, 2013.

[37] "Table a – 9," vol. 3, p. 1970, 1970.

[38] A. M. Aboghrara, B. T. H. T. Baharudin, M. A. Alghoul, N. M. Adam, A. A. Hairuddin, and H. A. Hasan, "Performance analysis of solar air heater with jet impingement on corrugated absorber plate," *Case Stud. Therm. Eng.*, vol. 10, no. May, pp. 111–120, 2017.

[39] G. Tanda, "Performance of solar air heater ducts with different types of ribs on the absorber plate," *Energy*, 2011.

[40] W. A. B. John A. Duffie, *Wiley: Solar Engineering of Thermal Processes, 4th Edition - John A. Duffie, William A. Beckman*. 2013.

[41] L. Bennamoun, "An Overview on Application of Exergy and Energy for Determination of Solar Drying Efficiency," *Int. J. Energy Eng.*, 2012.

[42] "Chapter 10b: The Psychrometric Chart (Updated 7/22/2014)." [Online]. Available: https://www.ohio.edu/mechanical/thermo/applied/chapt.7_11/chapter10b.html. [Accessed: 20-Mar-2019].

[43] S. Panchal, K. S. Solanki, S. Yadav, A. ilkar Kumar, and R. Nagaich, "Design, Construction and Testing of Solar Dryer with Roughened Surface Solar Air Heater," *Int. J. Innov. Res. Eng. Sci. ISSN*, 2013.

[44] F. K. Forson, M. A. A. Nazha, F. O. Akuffo, and H. Rajakaruna, "Design of mixed-mode natural convection solar crop dryers: Application of principles and rules of thumb," *Renew. Energy*, vol. 32, no. 14, pp. 2306–2319, Nov. 2007.

[45] A. S. Yadav and J. L. Bhagoria, "A CFD (computational fluid dynamics) based heat transfer and fluid flow analysis of a solar air heater provided with circular transverse wire rib roughness on the absorber plate," *Energy*, 2013.

[46] R. Tchinda, "A review of the mathematical models for predicting solar air heaters systems," *Renewable and Sustainable Energy Reviews*. 2009.

[47] D. A. Tzempelikos, A. P. Vouros, A. V. Bardakas, A. E. Filios, and D. P. Margaris, "Analysis of air velocity distribution in a laboratory batch-type tray air dryer by computational fluid dynamics," *Int. J. Math. Comput. Simul.*, vol. 6, no. 5, pp. 413–421, 2012.

[48] B. K. Bala and M. A. Hossain, *Solar drying of fishery products*. 2012.

[49] U. K. Neqas, S. Committees, and T. Of, "Appendix 1," pp. 909–949.

APPENDIX

A: Table A1-1: Typical checklist for evaluation and selection of solar dryers. [48]

	PARAMETER	FEATURES
1.	Physical features of dryer	✓ Type, size and shape ✓ Loading capacity (kg/ unit tray area) ✓ Loading/unloading convenience
2.	Thermal performance	✓ Drying period/time ✓ Drying efficiency ✓ Airflow rate ✓ Solar insolation
3.	Properties of the material being handled	✓ Physical characteristics (wet/dry) ✓ Particle size
4.	Drying characteristics of the material	✓ Type of moisture (bound, unbound or both) ✓ Initial moisture content ✓ Final moisture content ✓ Permissible drying temperature
5.	Product qualities	✓ Contamination ✓ Uniformity of final moisture content ✓ Appearance ✓ Flavor
6.	Economics	✓ Cost of dryer ✓ Cost of drying ✓ Payback
7.	Other parameters	✓ Ease of operation ✓ Safety and reliability ✓ Maintenance

B: Table A-22: Ideal gas properties of air[49]

TABLE A–9

Properties of air at 1 atm pressure

Temp. T, °C	Density ρ, kg/m³	Specific Heat c_p J/kg·K	Thermal Conductivity k, W/m·K	Thermal Diffusivity α, m²/s	Dynamic Viscosity μ, kg/m·s	Kinematic Viscosity ν, m²/s	Prandtl Number Pr
−150	2.866	983	0.01171	4.158×10^{-6}	8.636×10^{-6}	3.013×10^{-6}	0.7246
−100	2.038	966	0.01582	8.036×10^{-6}	1.189×10^{-6}	5.837×10^{-6}	0.7263
−50	1.582	999	0.01979	1.252×10^{-5}	1.474×10^{-5}	9.319×10^{-6}	0.7440
−40	1.514	1002	0.02057	1.356×10^{-5}	1.527×10^{-5}	1.008×10^{-5}	0.7436
−30	1.451	1004	0.02134	1.465×10^{-5}	1.579×10^{-5}	1.087×10^{-5}	0.7425
−20	1.394	1005	0.02211	1.578×10^{-5}	1.630×10^{-5}	1.169×10^{-5}	0.7408
−10	1.341	1006	0.02288	1.696×10^{-5}	1.680×10^{-5}	1.252×10^{-5}	0.7387
0	1.292	1006	0.02364	1.818×10^{-5}	1.729×10^{-5}	1.338×10^{-5}	0.7362
5	1.269	1006	0.02401	1.880×10^{-5}	1.754×10^{-5}	1.382×10^{-5}	0.7350
10	1.246	1006	0.02439	1.944×10^{-5}	1.778×10^{-5}	1.426×10^{-5}	0.7336
15	1.225	1007	0.02476	2.009×10^{-5}	1.802×10^{-5}	1.470×10^{-5}	0.7323
20	1.204	1007	0.02514	2.074×10^{-5}	1.825×10^{-5}	1.516×10^{-5}	0.7309
25	1.184	1007	0.02551	2.141×10^{-5}	1.849×10^{-5}	1.562×10^{-5}	0.7296
30	1.164	1007	0.02588	2.208×10^{-5}	1.872×10^{-5}	1.608×10^{-5}	0.7282
35	1.145	1007	0.02625	2.277×10^{-5}	1.895×10^{-5}	1.655×10^{-5}	0.7268
40	1.127	1007	0.02662	2.346×10^{-5}	1.918×10^{-5}	1.702×10^{-5}	0.7255
45	1.109	1007	0.02699	2.416×10^{-5}	1.941×10^{-5}	1.750×10^{-5}	0.7241
50	1.092	1007	0.02735	2.487×10^{-5}	1.963×10^{-5}	1.798×10^{-5}	0.7228
60	1.059	1007	0.02808	2.632×10^{-5}	2.008×10^{-5}	1.896×10^{-5}	0.7202
70	1.028	1007	0.02881	2.780×10^{-5}	2.052×10^{-5}	1.995×10^{-5}	0.7177
80	0.9994	1008	0.02953	2.931×10^{-5}	2.096×10^{-5}	2.097×10^{-5}	0.7154
90	0.9718	1008	0.03024	3.086×10^{-5}	2.139×10^{-5}	2.201×10^{-5}	0.7132
100	0.9458	1009	0.03095	3.243×10^{-5}	2.181×10^{-5}	2.306×10^{-5}	0.7111
120	0.8977	1011	0.03235	3.565×10^{-5}	2.264×10^{-5}	2.522×10^{-5}	0.7073
140	0.8542	1013	0.03374	3.898×10^{-5}	2.345×10^{-5}	2.745×10^{-5}	0.7041
160	0.8148	1016	0.03511	4.241×10^{-5}	2.420×10^{-5}	2.975×10^{-5}	0.7014
180	0.7788	1019	0.03646	4.593×10^{-5}	2.504×10^{-5}	3.212×10^{-5}	0.6992
200	0.7459	1023	0.03779	4.954×10^{-5}	2.577×10^{-5}	3.455×10^{-5}	0.6974
250	0.6746	1033	0.04104	5.890×10^{-5}	2.760×10^{-5}	4.091×10^{-5}	0.6946
300	0.6158	1044	0.04418	6.871×10^{-5}	2.934×10^{-5}	4.765×10^{-5}	0.6935
350	0.5664	1056	0.04721	7.892×10^{-5}	3.101×10^{-5}	5.475×10^{-5}	0.6937
400	0.5243	1069	0.05015	8.951×10^{-5}	3.261×10^{-5}	6.219×10^{-5}	0.6948
450	0.4880	1081	0.05298	1.004×10^{-4}	3.415×10^{-5}	6.997×10^{-5}	0.6965
500	0.4565	1093	0.05572	1.117×10^{-4}	3.563×10^{-5}	7.806×10^{-5}	0.6986
600	0.4042	1115	0.06093	1.352×10^{-4}	3.846×10^{-5}	9.515×10^{-5}	0.7037
700	0.3627	1135	0.06581	1.598×10^{-4}	4.111×10^{-5}	1.133×10^{-4}	0.7092
800	0.3289	1153	0.07037	1.855×10^{-4}	4.362×10^{-5}	1.326×10^{-4}	0.7149
900	0.3008	1169	0.07465	2.122×10^{-4}	4.600×10^{-5}	1.529×10^{-4}	0.7206
1000	0.2772	1184	0.07868	2.398×10^{-4}	4.826×10^{-5}	1.741×10^{-4}	0.7260
1500	0.1990	1234	0.09599	3.908×10^{-4}	5.817×10^{-5}	2.922×10^{-4}	0.7478
2000	0.1553	1264	0.11113	5.664×10^{-4}	6.630×10^{-5}	4.270×10^{-4}	0.7539

C: Psychrometric Chart

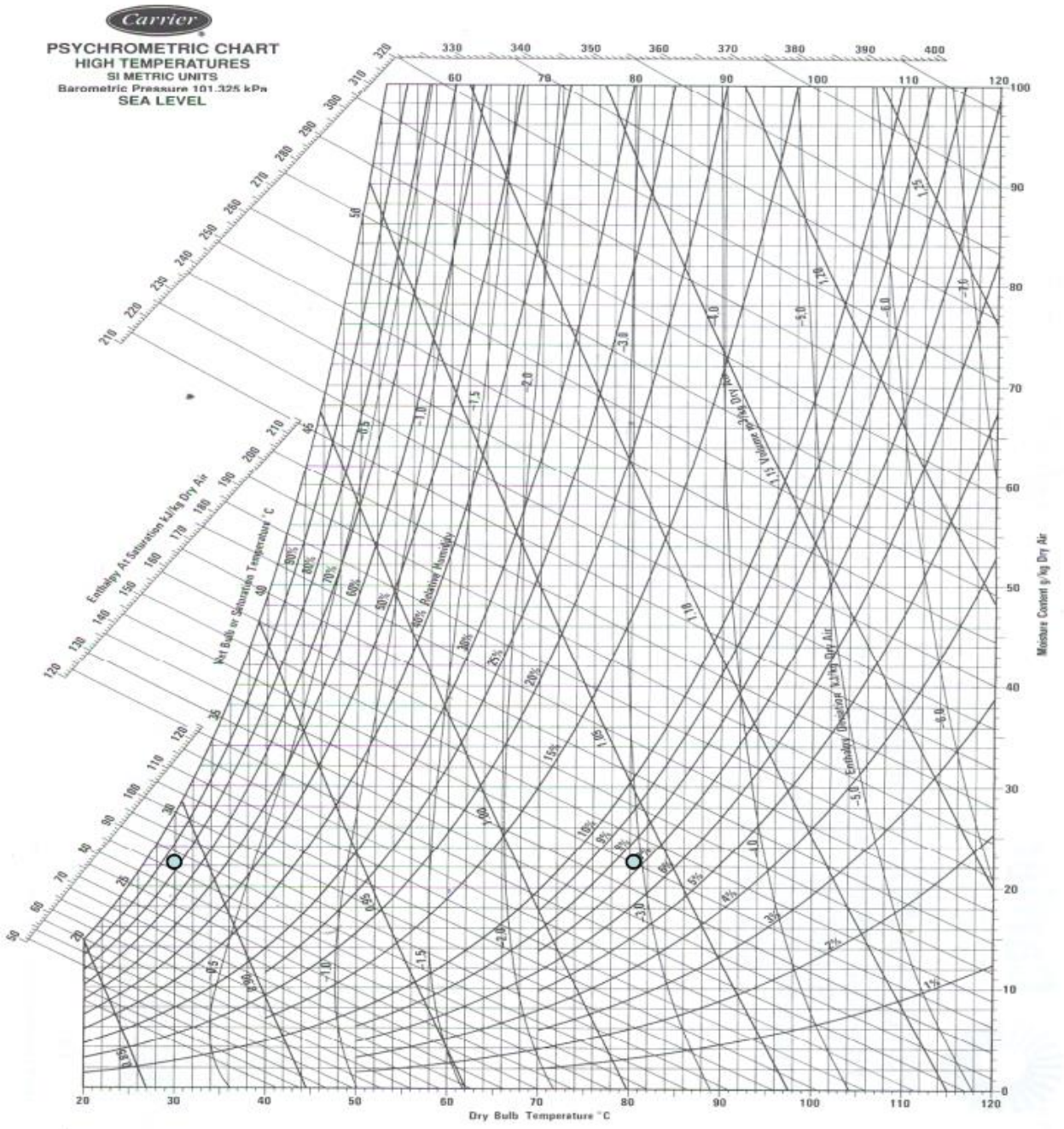

D: Mat lab code used to simulate solar radiation

```
function It=solarradiation(Gsc,fi,Llog,roug)
%It=solarradiation(1367,8.06,36.57,0.2)
Gsc=1367;% Gsc is the solar constant 1367W/m2
fi=8.06;% is the local geographical latitude ¦Õ
Llog=36.57;%  is the local geographical longitude
roug=0.2;% is the ground albedo with 0.2 for ground surface.
for n=1:365
    Gon(1,n)=Gsc*(1+0.033*cosd(360*n/365));
    delta(1,n)=23.45*sind(360*(284+n)/365);
    omigas(1,n)=acosd(tand(delta(1,n))*(-tand(fi)));

Ho(1,n)=24*3600*Gon(1,n)/pi*(cosd(fi)*cosd(delta(1,n))*sind(omigas(1,n))+2*pi
*omigas(1,n)/360*sind(fi)*sind(delta(1,n)));
    N(1,n)=2*omigas(1,n)/15;
    %---------------------------------------%
    if n<=31 && n>=1
        n1=6.4;
    elseif n>=32 && n<=59
        n1=7.2;
    elseif n>=60 && n<=90
        n1=7.7;
    elseif n>=91 && n<=120
        n1=8.5;
    elseif n>=121 && n<=151
        n1=9.0;
    elseif n>=152 && n<=181
        n1=8.5;
    elseif n>=182 && n<=212
        n1=7.0;
    elseif n>=213 && n<=243
        n1=7.5;
    elseif n>=244 && n<=273
        n1=8.2;
    elseif n>=274 && n<=304
        n1=7.5;
    elseif n>=305 && n<=334
        n1=6.1;
    else
        n1=5.9;
    end

    if (n>=1 && n<=59) || (n>=305 && n<=365)
        Kt(1,n)=0.14+0.47*n1/N(n);
    elseif n>=152 && n<=243
        Kt(1,n)=0.24+0.4*n1/N(n);
    else
        Kt(1,n)=0.36+0.23*n1/N(n);
    end
   %-----------------------%

   H(1,n)=Ho(1,n)*Kt(1,n); %

   %------------%
```

```
   if Kt(1,n)<=0.17
       Hd(1,n)=0.99*H(1,n);
   elseif Kt(1,n)>0.17 && Kt(1,n)<0.75
        Hd(1,n)=(1.188-2.272*Kt(1,n)+9.473*(Kt(1,n))^2-
21.865*(Kt(1,n))^3+14.648*(Kt(1,n))^4)*H(1,n);
   elseif Kt(1,n)>0.75 && Kt(1,n)<0.18
        Hd(1,n)=(0.632-0.54*Kt(1,n))*H(1,n);
   else
       Hd(1,n)=0.2*H(1,n);
   end
   %---------------%

   for h=1:24
       m=24*(n-1)+h;
       tttt(1,m)=m;
       omiga(1,m)=15*((h*60+9.87*sind(2*360*(n-81)/364)-7.53*cosd(360*(n-
81)/364)-1.5*sind(360*(n-81)/364)-4*(120-Llog))/60-12);

       if abs(omiga(1,m))<omigas(1,n)
          m1=m;
          m2=m+1;
          omiga(1,m1)=omiga(1,m);
          omiga(1,m2)=15*(((h+1)*60+9.87*sind(2*360*(n-81)/364)
7.53*cosd(360*(n-81)/364)-1.5*sind(360*(n-81)/364)-4*(120-Llog))/60-12);
          % I is Hourly global solar radiation on the horizontal surface
          I(1,m)=(H(1,n)*pi/24*((0.409+0.5016*sind(omigas(1,n)-60))+(0.6609-
0.4767*sind(omigas(1,n)-
60))*cosd((omiga(1,m1)+omiga(1,m2))/2))*(cosd((omiga(1,m1)+omiga(1,m2))/2)-
cosd(omigas(1,n)))/(sind(omigas(1,n))-
2*pi*omigas(1,n)*cosd(omigas(1,n))/360))/3600;
          % Id is Hourly diffuse solar radiation on the horizontal surface
          Id(1,m)=(Hd(1,n)*pi/24*(cosd((omiga(1,m1)+omiga(1,m2))/2)-
cosd(omigas(1,n)))/(sind(omigas(1,n))-
2*pi*omigas(1,n)*cosd(omigas(1,n))/360))/3600;
          % Rbave is Ratio of beam radiation on tilted surface to that on
horizontal surface
          Rbave(1,m)=(cosd(delta(1,n))*(sind(omiga(1,m2))-
sind(omiga(1,m1)))/(cosd(fi)*cosd(delta(1,n))*(sind(omiga(1,m2))-
sind(omiga(1,m1)))+sind(fi)*sind(delta(1,n))*pi/180*(omiga(1,m2)-
omiga(1,m1))))/3600;

cosd(fi))/2+Rbave(1,m))+Id(1,m)*((1+cosd(fi))/2-Rbave(1,m));% Hourly global
solar radiation on the tilted surface
       if It(1,m)<0
           It(1,m)=0;
       end
       if I(1,m)<0
           I(1,m)=0;
       end
       if Id(1,m)<0
           Id(1,m)=0;
       end
   end
```

```
end

subplot(2,2,1)
plot(tttt,It)
title('Hourly global solar radiation on the tilted surface')
xlabel('time(h)')
ylabel('It(W/m2)')
grid on
hold on
subplot(2,2,2)
plot(tttt,I)
title('Hourly global solar radiation on the horizontal surface')
xlabel('time(h)')
ylabel('I(W/m2)')
grid on
hold on
subplot(2,2,3)
plot(tttt,Id)
title('Hourly diffuse solar radiation on the horizontal surface')
xlabel('time(h)')
ylabel('Id(W/m2)')
grid on
subplot(2,2,4)
plot(tttt,Rbave)
title('Ratio of beam radiation on tilted surface to that on horizontal
surface')
xlabel('time(h)')
ylabel('Rbave')
grid on
```

E.EES code to find ideal gas property of air

```
"Knowns-units set to J,K,kPa"
Hc=0.02 [m];
ep=0.95;
Ta=300 [K];
hw=13.6;
Patm=101.3 [kPa];
Tap=105[K]
theta=18.06[degree];
eg=0.88;
Tc=54.10
sigma=5.67*10^(-8);
ec=0.89;
g=g#
"get property at Tm"
Tm=(Tap+Tc)/2
miw=viscosity(air, T = Tm);
 k = conductivity(air, T = Tm)
Cp = specheat(air, T = Tm);
roh=density(air, T =Tm,P=Patm)
v=miw/roh;
alpha=k/(roh*Cp)
Pr=Prandtl(air, T = Tm);
```